Biophysical Reviews
https://doi.org/10.1007/s12551-022-00999-7

REVIEW

# Membrane attachment and fusion of HIV-1, influenza A, and SARS-CoV-2: resolving the mechanisms with biophysical methods

Geetanjali Negi[1] · Anurag Sharma[1] · Manorama Dey[1] · Garvita Dhanawat[1] · Nagma Parveen[1]

Received: 22 July 2022 / Accepted: 16 September 2022


## Abstract

Attachment to and fusion with cell membranes are two major steps in the replication cycle of many human viruses. We focus on these steps for three enveloped viruses, i.e., HIV-1, IAVs, and SARS-CoV-2. Viral spike proteins drive the membrane attachment and fusion of these viruses. Dynamic interactions between the spike proteins and membrane receptors trigger their specific attachment to the plasma membrane of host cells. A single virion on cell membranes can engage in binding with multiple receptors of the same or different types. Such dynamic and multivalent binding of these viruses result in an optimal attachment strength which in turn leads to their cellular entry and membrane fusion. The latter process is driven by conformational changes of the spike proteins which are also class I fusion proteins, providing the energetics of membrane tethering, bending, and fusion. These viruses exploit cellular and membrane factors in regulating the conformation changes and membrane processes. Herein, we describe the major structural and functional features of spike proteins of the enveloped viruses including highlights on their structural dynamics. The review delves into some of the case studies in the literature discussing the findings on multivalent binding, membrane hemifusion, and fusion of these viruses. The focus is on applications of biophysical tools with an emphasis on single-particle methods for evaluating mechanisms of these processes at the molecular and cellular levels.

**Keywords** HIV-1 · IAVs · SARS-CoV-2 · Virions · Spike protein · Structural conformations · Binding affinity · Multivalent binding · Hemifusion · Fluorescence imaging · Force spectroscopy · Cellular factors

## Introduction

Viruses are infectious particles with a diameter of ~ 50–500 nm. A virus particle includes the viral genome (RNA or DNA) encapsulated in a capsid representing a protein shell (Fig. 1A–C). The capsid of an enveloped virus is further coated with a lipid bilayer. Though constituted of essential species of life (nucleic acid, protein, and lipid), viruses require the resources and machinery of host cells for their replication. The viral replication is a multistep process that can be generalized as follows: attachment to a host cell surface, specific interaction with the plasma membrane receptors, entry or penetration into the host cell including fusion with or encapsulation by the cellular membrane, capsid uncoating, release of the viral genome, genome replication, expression of viral proteins, assembly of the viral proteins and genomes into new virions, and their release from the host cell (Fig. 1D). Decades of studies by virologists, molecular and structural biologists, biophysicists, and researchers from interdisciplinary sciences have enabled us to gain molecular understanding and cellular pathway of these steps (Mercer et al. 2010; Friedrich et al. 2011; Belouzard et al. 2012; Merk and Subramaniam 2013; Ivanovic and Harrison 2015; Dou et al. 2018; Lu et al. 2020; V'kovski et al. 2021; Zhdanov 2021). Herein, we focus on two major steps in the replication of enveloped viruses, i.e., attachment to and fusion with host cell membranes. Earlier, this subject was reviewed by Helenius et al. (2018), White and Whittaker (2016), Melikyan (2011), Harrison 2005, Tang et al. (2020), Koehler et al. (2020), Jackson et al. (2022), and other researchers (Belozard et al. 2012; de Vries et al. 2020). We have focused on some of the biophysical studies

Geetanjali Negi, Anurag Sharma, and Manorama Dey contributed equally to the work.

✉ Nagma Parveen
nagma@iitk.ac.in

[1] Department of Chemistry, Indian Institute of Technology Kanpur, Kanpur, India

Published online: 11 October 2022

in this review. In particular, we have compiled and discussed the existing findings on the membrane attachment and fusion of three major enveloped viruses which are human immunodeficiency virus 1 (HIV-1), influenza A viruses (IAVs), and severe acute respiratory syndrome coronavirus 2 (SARS-CoV-2). The major surface protein, also known as spike protein, of the virions drives the membrane attachment and fusion (Fig. 1). Although these virions are different in their genome type (according to Baltimore classification) and poly-protein structure, their spike proteins have structural homology and common functionality as class I fusion proteins. This makes them interesting candidates for a comparative analysis of the membrane attachment and fusion process of enveloped virions.

In the past few decades, the world has witnessed pandemics of infectious diseases caused by HIV-1, IAVs, and SARS-CoV-2. HIV-1 transmits via fluid exchange from infected hosts, whereas IAVs and SARS-CoV-2 transmit through droplets or aerosol that are released from infected hosts. While the infectious virions spread into different organs and tissues of a host upon transmission, the infection occurs only in specific organs or tissues of the host. This means that the infection is specific to host cell types as often expressed as host cell tropism. At the cellular level, the first step of viral replication is the interaction between virions and the host cell surface. For this, the virions must navigate through the crowded cell surface and attain an interaction with molecules which are either abundant or specific to the host cell. This is a complex task as the cell surface is rich in glycans, membrane receptors, glycolipids, etc. which can engage in a range of molecular interactions with the viral spike proteins. Here, the molecular structures are central in

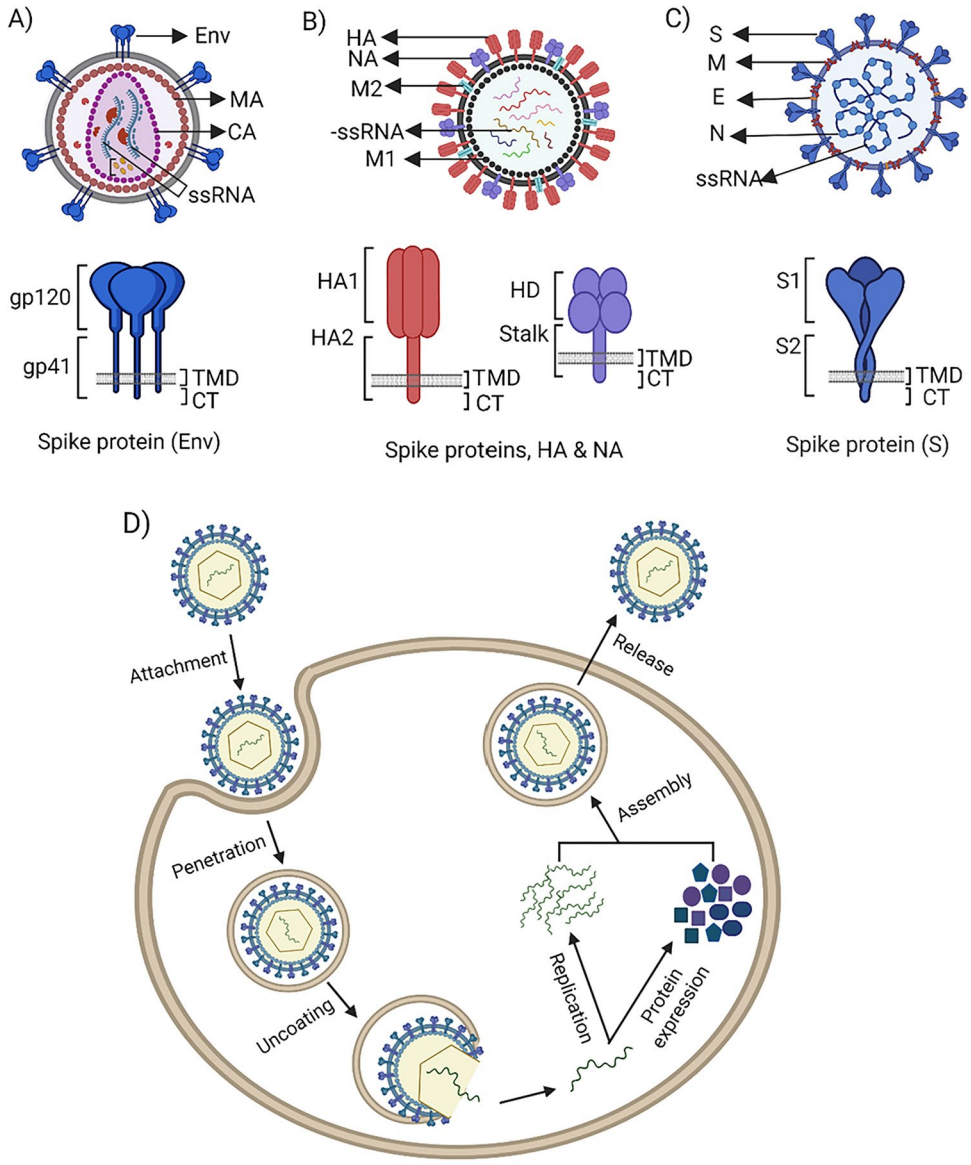


**Fig. 1** Schematics of **A** HIV-1, **B** IAV, and **C** SARS-CoV-2 virions including illustrations of their spike proteins. The head subunit of Env, HA, and the S protein is gp120, HA1, and S1, respectively. Similarly, the stalk subunit is gp41, HA2, and S2, respectively. The RBD and FP of the virions reside in the head and stalk subunit of the spike proteins, respectively. According to the Baltimore classification, the genome of HIV-1, IAVs, and SARS-CoV-2 is of Group VI, V, and IV, respectively. **D** Scheme showing the replication steps of the viruses in a host cell. TMD: transmembrane domain; CT: cytoplasmic tail; RBD: receptor binding domain; FP: fusion peptide; MA: matrix protein; CA: capsid protein; gp: glycoprotein of HIV-1; HA: hemagglutinin; NA: neuraminidase; M1 and M2: matrix proteins (proton channel) of IAVs; S: spike protein; M: membrane protein; E: envelope protein; N: nucleocapsid protein of SARS-CoV-2. Created with Biorender.com

determining the specificity and strength of the interaction. In a way, the structure and function of the spike proteins are interlinked. This is also why structural studies are an integral part of virology and have been critical for the development of antivirals and vaccines.

At the cell surface, the virions come across a ~ 0.5–1.5-µm-thick layer of transmembrane proteoglycans and mucins which are rich in glycans, and the spike proteins interact with the glycans. The glycans are reported to act as binding moieties, decoy agents, or steric barriers to the virions (De Vries et al. 2012; Connell and Lortat-Jacob 2013; McAuley et al. 2017; Clausen et al. 2020; Liu et al. 2021). In some cases, the dynamic binding between the spike proteins and glycans enables the virions to migrate through them and reach the plasma membrane, making the glycans act as attachment factors of the viruses, whereas a relatively strong interaction between the spike proteins and specific glycans may cause trapping of the virions.(Fig. 2)

At the plasma membrane, the spike protein engages in a specific binding with membrane receptors leading to the membrane attachment of the virions on host cells (de Vries et al. 2020; Koehler et al. 2020; Llorente García and Marsh 2020; Shang et al. 2020a; Zhou et al. 2020; Jackson et al. 2022) (Fig. 1D). Typically, a conserved site on the head subunit of the spike protein (Figs. 2, 5, and 8), known as receptor binding domain (RBD), interacts with a specific receptor via multiple non-covalent bonds forming an RBD–receptor pair. The equilibrium dissociation constant ($k_D$) of such a pair expresses the receptor binding affinity. The spike proteins of HIV-1, IAVs, and SARS-CoV-2 are oligomeric. This means a single spike protein has multiple RBDs and can form multiple RBD–receptor pairs depending on the protein structure, its conformational dynamics and receptor binding affinity, etc. (Chang et al. 2005; Kwon et al. 2012; Benton et al. 2020b; Walls et al. 2020; Wrapp et al. 2020). Therefore, finding the primary receptor(s), resolving the structure of the spike protein–receptor complex, and determining the corresponding binding affinity or avidity values are of major importance for emerging strains of HIV-1, IAVs, and SARS-CoV-2 viruses (Takemoto et al. 1996; Myszka et al. 2000; Shang et al. 2020a, b; Wrapp et al. 2020).

However, the binding affinity (as typically expressed with $k_D$) or avidity of spike proteins does not represent the overall attachment strength of intact virions on the plasma membrane. It is because of two major reasons: (1) a single virion contains multiple spike proteins either of the same or different functional types (Harris et al. 2006; Zhu et al. 2006; Ke et al. 2020) (Fig. 1A–C), and (2) multiple receptors and co-receptors can be accommodated within the membrane contact area of a virion (Floyd et al. 2008; Zhdanov and Höök 2015; Pak et al. 2022). This means a single virion can engage in interaction with multiple receptors, co-receptors, and other membrane factors on the plasma membrane (Figs. 4B, 6C, and 9A). This is typically described as multivalent binding of viruses (Müller et al. 2019; Parveen et al. 2019; de Vries et al. 2020; Yang et al. 2020; Pak et al. 2022). It is well accepted in the literature that the virions exploit binding of this type for increasing their residence time and attaining an optimal attachment on the plasma membrane (Sakai et al. 2017; Müller et al. 2019; Shaik et al. 2019).

The membrane attachment of the virions leads to their cellular internalization (Fig. 1D). This can occur either via fusion of the bound virions on the plasma membrane or upon their endocytosis followed by membrane fusion in early/late endosomes (Melikyan 2011; White and Whittaker 2016; Tang et al. 2020). A highly conserved residue, i.e., fusion peptide (FP), residing in the stalk subunit of the spike protein is the key element for membrane fusion (Figs. 3, 6, and 8). A conformational transition (pre-fusion to pre-hairpin) of the spike protein causes the head subunit to move away and the sequestered FP to become available for insertion into a target membrane. This leads to the tethering of the viral envelope with the target cell membrane (Figs. 4B, 7D, and 10D). An energetically favorable conformational transition (pre-hairpin to hairpin) of the protein causes the tethered membranes to bend and, finally, merge/fuse. While these conformational transitions of the spike protein drive the fusion process, the fusion kinetics at the virion and cellular level may have more complex features and other associated interactions.

A range of analytical and biophysical techniques have been employed by virologists and biophysicists to resolve the molecular and cellular mechanism of the membrane attachment and fusion of the enveloped viruses under consideration (Harrison 2008; Hamilton et al. 2012; Parveen et al. 2018; Liu et al. 2020; Bally et al. 2021). Biochemical methods like enzyme-linked immunoassay and biophysical ensemble-averaged techniques like surface plasmon resonance (SPR) have been widely applied in characterizing the spike proteins and evaluating their binding affinity to membrane receptors (Myszka et al. 2000; Suenaga et al. 2012; Kim et al. 2020; Walls et al. 2020). In recent years, single-molecule and single-particle techniques have gained popularity in virus research (Howard and Munro 2019; Liu et al. 2020). These techniques provide information about structure, molecular interactions, and, more importantly, structural and functional heterogeneity. For example, single-particle imaging with cryo-electron microscopy (cryo-EM) and electron tomography (cryo-ET) techniques has been a tremendous success in resolving the structure and configurational dynamics of the spike proteins and finding out their binding sites toward receptors, coreceptors, and antibodies (Liu et al. 2008; Lee 2010; Mao et al. 2013; Merk and Subramaniam 2013; Calder and Rosenthal 2016; Benton et al. 2020a; Henderson et al. 2020; Li et al. 2020; Walls et al. 2020; Wrapp et al. 2020). More specialized single-molecule

techniques like atomic force microscopy (AFM) have also been applied to determine the binding affinity of spike proteins and explore the multivalent binding of virions on cell surface (Chang et al. 2005; Delguste et al. 2018; Yang et al. 2020). Advanced fluorescence microscopy techniques with single-molecule or single-particle sensitivity have been employed to resolve configurational dynamics of spike proteins in real time, trace the membrane attachment and fusion at single virion level, and image fusion pathways in host cells (Miyauchi et al. 2009; Yang et al. 2016, 2017; Das et al. 2018, 2021; Müller et al. 2019). Biomimetic platforms and model host cells in combination with single-particle imaging are applied for examining the heterogeneity and dynamics of virus attachment and fusion, and in exploring molecular factors that can influence these processes (Floyd et al. 2008; Miyauchi et al. 2009; Sakai et al. 2017; Clausen et al. 2020; Villamil Giraldo and Kasso 2020). A major aim of these imaging studies is to understand how the heterogeneity, dynamics, and molecular factors contribute to the cellular infection caused by these viruses. The readers are referred to reviews by Matrosovich et al. (2012), Schasfoort (2017), Murali et al. (2022), Murata and Wolf (2018), Zlatanova et al. (2000), Shashkova et al. (2017), and Parveen et al. (2018) for the detailed description of the operating principles of the above-mentioned biophysical techniques and their accuracy, resolutions (spatial and temporal), advantages, and limitations.

In this review, we have focused on the applications of biophysical methods at single-molecule and single-particle levels for studying the mechanisms of the membrane attachment and fusion of HIV-1, IAVs, and SARS-CoV-2 at the molecular and cellular levels. We have begun the review by describing the major structural features of the spike proteins including the conformational dynamics of the protein pertinent to the receptor binding and membrane fusion. Thereafter, we have discussed some of the reported studies with emphasis on the multivalent binding and membrane fusion kinetics of the virions at single-particle and cellular levels. To achieve a comprehensive yet compact discussion, we have limited our discussion to a few case studies and highlighted the applications of single-particle and single-molecule imaging techniques.

## Human immunodeficiency virus 1

HIV-1 is the causative agent of acquired immune deficiency syndrome (AIDS) that weakens the human immune system and causes the development of other infectious or cancerous diseases. AIDS was first identified in 1981 in Central Africa and since then it has affected an estimated 79.3 million people and more than 37.7 million people living with HIV-1 infection globally (Sharp and Hahn 2011). The disease pathogenesis indicates that HIV-1 effectively counteracts the human immune system and infects major immune cells, i.e., $CD4^+$ T lymphocytes, macrophages, and dendritic cells (Chinen and Shearer 2002; Simon et al. 2006). Because of the high mutation rate and viral turnover, HIV-1 has been genetically detruncated into four branches such as M, O, N, and P. Majority of the global AIDS pandemic is due to the M subtype which is also subdivided into 10 groups (Rashid et al. 2022). This genetic diversity of HIV-1 causes difficulty in the fruitful design of the AIDS vaccination, diagnosis, and antiretroviral therapy.

In general, HIV-1 belongs to the genus *Lentivirus* within the family of *Retroviridae*. It has two identical copies of a positive-sense single-stranded RNA strand with a length of ~ 9.3 kilobases (kb) encapsulated in the viral capsid that is further enveloped by a lipid bilayer, forming a spherical particle of ~ 100 nm in diameter (Fig. 1A). The HIV-1 genome is reverse transcribed to DNA in host cells and contains three major polyprotein-coding genes: structural (*gag*, *pol*, *env*), two regulatory (*tat*, *rev*), and four accessories (*nef*, *vif*, *vpr*, *vpu*) (Prabakaran et al. 2007). The four *gag* encoded proteins, i.e., matrix (MA), capsid (CA), nucleocapsid (NC), and p6, form the core of the virion. The four *pol* encoded proteins are the essential viral enzymes, i.e., reverse transcriptase (RT), protease, and integrase. The RT reverse transcribes the viral RNA into DNA and the protease cleaves the viral polyproteins (Gag, Pol) into individual gene products. Among the structural components, the transmembrane glycoprotein (TM, gp41) and surface glycoprotein (SU, gp120) are the two major *env* encoded proteins (Fig. 1A).

The gp120 binds to cluster of differentiation 4 (CD4) and chemokine receptors, in particular, CXCR4 and CCR5 of the plasma membrane. CD4 is the primary receptor of HIV-1. CXCR4 or CCR5 is the co-receptor of the virus depending on the cell tropism and pathogenesis. The gp41 protein drives the fusion between the viral envelope and a cell membrane. These viral glycoproteins form a complex (via non-covalent interactions) that is named Env or, in general, spike protein of the virus (Fig. 1A). The architecture of Env comes from its spike head (10–15 nm wide) made of gp120, a relatively short stalk (~ 10 nm) made of gp41, and a central void surrounding a C3 axis (Mao et al. 2013). Cryo-ET data reveal that HIV-1 has $14 \pm 7$ Env spikes per particle (Zhu et al. 2006) which are fewer compared to that of other enveloped viruses like influenza (350–400) (Harris et al. 2006). Irrespective of the lower surface density, Env protein is a major target of neutralizing antibodies (NAbs) generated by the human immune system (Kwong et al. 1998; Caillat et al. 2021). This is because of the surface protrusion of the protein, exposing it by ~ 10 nm from the virus envelope. The functions and immunogenicity of Env make them

a major target of antiviral drugs and it is a suitable candidate for vaccine development.

**Structure and configurational dynamics of gp120** The Env (M.W. of 160 kDa) of HIV-1 is a trimeric viral transmembrane protein. Each monomer of Env consists of 840–860 amino acids (aa) among which 345 aa form gp41 and the rest form gp120 (Kwong et al. 1998; Liu et al. 2008; Mao et al. 2013) (Fig. 2A). The glycoproteins are formed upon an enzymatic cleavage (via furin or furin-like proteases) of the viral gp160 in host cells (Hellengerger et al. 1992). The amino acid sequence of gp120 is less conserved than that of gp41. Structures of the full-length and truncated (core) gp120 are resolved using both cryo-EM (Liu et al. 2008; Mao et al. 2013) and X-ray crystallography (Kwong et al. 1998; Kwon et al. 2012, 2015). Each gp120 monomer (deglycosylated size, $50 \times 50 \times 25$ Å$^3$) contains three domains: outer domain, inner domain, and trimer association domain (TAD) (Fig. 2B). The structure of inner and outer domains is dominated by β-sheets and loops. The TAD connects the inner and outer domains of the adjacent gp120 monomers in the trimeric protein.

The Env protein goes through conformational changes upon binding to CD4 and CCR5/CXCR4 (Pancera et al. 2010), triggering essential steps or processes to commence the cellular internalization and membrane fusion of HIV-1 (Melikyan 2011). Also, the majority of NAbs bind to the unliganded (not bound to a receptor) Env, meaning the unliganded Env conformations can be suitable vaccine candidates (immunogens). Hence, there has been an intense focus on resolving the liganded (Kwong et al. 1998; Liu et al. 2008; Harris et al. 2011; Tran et al. 2012; Mao et al. 2013) and unliganded conformations (Liu et al. 2008; Harris et al. 2011; Kwon et al. 2012, 2015; Mao et al. 2013; Munro et al. 2014; Li et al. 2020; Mangala Prasad et al. 2022) of Env, and understanding the structural dynamics of the protein. Early in 1998, Kwong et al. (1998) solved the crystal structure of monomeric gp120 core complexed with CD4 at a resolution of 2.5 Å. The authors proposed that the gp120 monomer consists of 25 β-strands and 5 α-helices, and indicated the relative positions of variable loops (V1–V5). The inner domain contains two helices and a two-strand bundle with a small five-stranded β-sandwich. The outer domain is made up of a six-stranded mixed directional β-sheet which clamps with α-2 helix and a seven-stranded antiparallel β-barrel. The V1–V2, V4–V5, and V3 loops are associated with the inner domain, the outer domain, and TAD, respectively (Fig. 2B, C). The inner and outer domain is outlined by a four-stranded bridging sheet (blue/green β2/β3 and yellow/orange β20/β21 in Fig. 2C). The CD4 binds at the interface of the outer domain, inner domain, and bridging sheet. Because of the mismatch in the surface topography, the actual contact area between the gp120 monomer and CD4 receptor is rather small. About 26 amino acid residues of gp120 interact with 22 residues of CD4, forming 12 H-bonds and several Van der Waals interactions. Crystallography structures resolved by Kwon et al. (2012, 2015) indicate that the liganded and unliganded gp120 resemble closely. The authors observed that the CD4-binding results in conformational movement of the inner domain (4 Å) and bridging sheet (10 Å) whereas the outer domain (2 Å) is weakly altered.

The application of cryo-EM and cryo-ET techniques has accelerated the structural analysis (6–15 Å resolution) of the soluble Env (Harris et al. 2011; Tran et al. 2012; Mao et al. 2013) and Env embedded on intact virions (Liu et al. 2008; Li et al. 2020; Mangala Prasad et al. 2022). Cryo-EM data of Mao et al. (2013) show that different regions of the inner domain go through conformational changes in a layered manner upon the binding of gp120 to CD4. In particular, β-sandwich and different helices of the inner domain rotate by ~ 60° and ~ 40–110°, respectively, compared to the more or less fixed outer domain. It is to mention that there has been a debate over the resolved structures in this article. Liu et al. (2008) employed Cryo-ET to visualize the structure of trimeric gp120 on intact virions. The authors reported that each gp120 monomer rotates ~ 45° around an axis parallel to the C3-axis and has an out-of-plane rotation by ~ 15° upon the CD4 binding. At the bound state of gp120, the V3 loop of the outer domain exposes to the Env surface (encircled in Fig. 2C) and becomes accessible for interaction with the co-receptors. Huang et al. (2005) and others (Masso and Vaisman 2010) resolved the interaction sites of the V3 base with the N terminus of CCR5. From the structure and sequence analysis, Huang et al. concluded that HIV-1 binds with CXCR4 if the 11th and 25th positions of V3 are positively charged. Otherwise, HIV-1 uses CCR5 as its co-receptor.

Unlike the crystallography and electron microscopy techniques, single-molecule fluorescence resonance energy transfer (smFRET) coupled with fluorescence microscopy technique is a suitable method for tracing the real-time conformational dynamics of spike proteins. Munro et al. (2014), Lu et al. (2019), Ma et al. (2018), and others have analyzed FRET signals from single HIV-1 particles upon fluorescence labeling of specific sites (V1 and V4) of the gp120 protein. The authors reported that the gp120 has three dynamic conformations. While the protein is predominately at a closed conformation (low FRET), the CD4 binding causes a shift toward an open conformation. Interestingly, the binding of CD4 and a co-receptor mimic (17b) leads to an intermediate configuration, indicating a two-step activation of HIV-1 Env upon binding to the receptor and co-receptor (Munro et al. 2014).

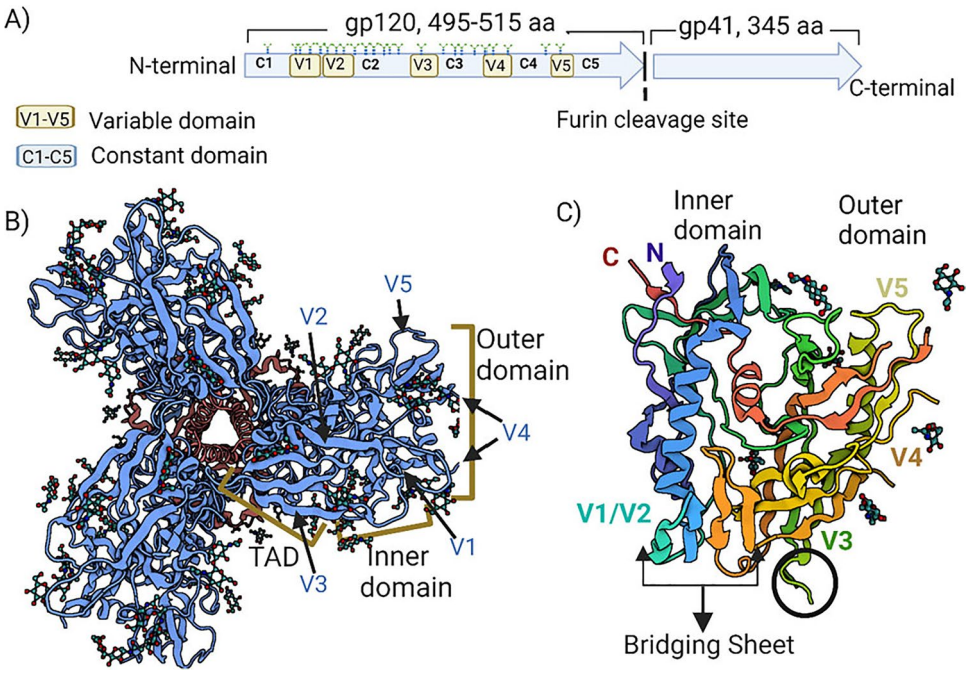


**Fig. 2** Structure of Env and the gp120 core. **A** Diagram of the sequence and major domains of Env showing the gp120 and gp41 subunits and the constant and variable domains of the gp120. **B** Top view of the tertiary structure of unliganded Env trimer (PDB ID: 4ZMJ; crystal structure at 3.31 Å resolution (Kwon et al. 2015). The gp120 and gp41 are color coded in blue and dark orange, respectively. Inner, outer, and trimer association domains of gp120 are indicated with brackets. **C** The tertiary structure of gp120 core at unliganded state (PDB ID: 3TGQ, crystallography structure at 3.4 Å resolution (Kwon et al. 2012). The interface between the inner, outer, and bridging sheet is the binding area of CD4 (Kwong et al. 1998). The encircled area at the V3 loop is the binding site of CCR5/CXCR4 co-receptor. The structure is shown in multi-color to highlight the domains and receptor binding region or interface. V (V1–V5): variable domain (1–5); C (C1–C5): constant domain (1–5); TAD: trimer association domain. Created with Biorender.com

**Binding affinity of gp120 to the membrane receptors** HIV-1 binds to the plasma membrane of host cells upon the interaction of Env/gp120 protein with membrane CD4 and CCR5/CXCR4 (Fig. 4A). Although the probable binding sites (bond formation) can be determined or estimated from their resolved structures (Fig. 2C), an accurate determination of the corresponding binding strength requires evaluation of the hydration effect and, more importantly, the dynamic nature of the interactions. Ensemble-averaged techniques like SPR and single-molecule/particle approaches like AFM and fluorescence microscopy have been applied by researchers for determining the binding affinity of gp120 toward CD4, CCR5/CXCR4 at the native or near-native condition, and further understand the dynamics of HIV-1 binding on the plasma membrane (Endreß et al. 2008).

Myszka et al. determined the affinity of the trimeric gp120 toward CD4 by evaluating their binding thermodynamics and kinetics which were traced using ensemble-averaged titration microcalorimetry and SPR techniques (Myszka et al. 2000). The titration data reveal that CD4 forms a 1:1 complex with the core gp120, and the corresponding binding enthalpy $\Delta H^{\circ}$ and entropy change $(-T\Delta S^{\circ})$ is $-63$ and 52 kcal/mol, respectively. This data indicates that a large number of bonding interactions (low $\Delta H^{\circ}$) is involved per gp120–CD4 pair but at an entropic cost. In other words, the binding leads to a substantial loss in the degrees of freedom. The SPR data even reveals how specific structural components of gp120 influence its binding strength toward CD4. The authors reported a binding affinity ($k_D$) of $22 \pm 6$ nM and $220 \pm 40$ nM for CD4 toward the full-length gp120 and core gp120, respectively. The core gp120 lacks 52 and 19 aa residues at the N terminus and C terminus, respectively, and this could explain the lower affinity of the core protein. Interestingly, this lowering comes from an increased dissociation rate as the $k_d$ or $k_{off}$ is an order of magnitude higher for core gp120 compared to that of the full-length protein. This indicates that the particular amino acid residues affect the binding dynamics between CD4 and gp120.

Similar binding experiments at the single-molecule level provide the distribution of the binding affinity and other allied binding parameters. Chang et al. (2005) employed the single-molecule force spectroscopy technique for determining various molecular parameters such as dissociation rate constant ($k_{off}$ or $k_d$), lifetime ($\tau$), and tensile strength ($x_B$) of gp120–CD4 and gp120–CCR5 pairs. The authors traced force curves upon the retraction of gp120-coated AFM tips on the surface of live cells that express CD4 or CCR5 or both in the plasma membrane, and from that they measured

the rupture force of gp120–CD4 and gp120–CCR5 pairs (Fig. 4C). Although the rupture force (~ 26 pN) is much lower compared to common adhesive proteins (~ 80 pN for p-selectin) (Hanley et al. 2003), the force data confirms that gp120 has a specific interaction with membrane CD4. Also, it interacts with membrane CCR5 only in the presence of either membrane CD4 or solubilized CD4 (sCD4). The $k_{off}$ of gp120–CD4, gp120–CCR5(CD4), and gp120–CCR5(sCD4) pairs is 4.1 $s^{-1}$ ($\tau \sim 0.24$ s), 0.7 $s^{-1}$ ($\tau \sim 1.42$ s), and 1.3 $s^{-1}$ ($\tau \sim 0.77$ s), respectively. This data indicates that gp120 has more dynamic interaction (shorter lifetime) with membrane CD4 in the absence of CCR5 co-receptor. Chang et al.'s data indicates that the viral protein must bind to both CD4 and CCR5 to attain a higher lifetime (lower $k_{off}$) of the complex (Fig. 4B-i). Such multivalent interaction of gp120 can explain the requirement of co-receptor for HIV-1 binding. Also, it helps to understand how HIV-1 can attain an adequate attachment strength on the plasma membrane irrespective of having a relatively low surface density of Env.

**Dynamic binding of HIV-1 particles to the glycans and membrane receptors** The high affinity yet dynamic binding of gp120 to CD4, CCR5, and/or other attachment factors regulate the attachment and lateral dynamics of HIV-1 particles on cell membranes (Steffens and Hope 2004; Lampe et al. 2007; Endreß et al. 2008). Single-particle fluorescence imaging techniques have been at the disposal to probe such dynamics (Lampe et al. 2007). For example, Endreß et al. (2008) applied the single virus tracking (SVT) approach to evaluate the diffusion and immobilization pattern of HIV-1 on cell surfaces. The authors recorded time-lapse images of fluorescently tagged HIV-1 pseudovirions (MA and Vpr are labeled with fluorescent proteins using genetic engineering) on live cells using wide-field fluorescence microscopy. The corresponding single-particle trajectories show that a single virion makes consecutive contacts with a cell surface. About 20% of these contacts lead to immobilization of HIV-1 without any cellular internalization or membrane fusion. The immobilized virus fraction neither changes upon blocking of CD4 nor influences the cellular infection. Interestingly, the immobilization linearly increases with increasing heparan-linked proteoglycans (HSPGs) expression on cell surfaces. The rest of the virus particles (80%) are diffusive and make transient contacts (< 240 ms) with the plasma membrane. The average contact time of the diffusive HIV-1 particles is 49 ms and 24 ms for cells with and without CD4, respectively. Together, these virus mobility data indicate that proteoglycans partially block HIV-1 passage to the plasma membrane and CD4 receptors are essential for HIV-1 to attain sufficient residence time (> 40 ms) on the plasma membrane (Fig. 4A). The data of Endreß et al. show that the cell surface proteoglycans act as trapping agents for HIV-1 and the receptor-bound virions have lateral mobility with a sufficient residence time.

**Structure and configurational transition of gp41** It is well established that HIV-1 particles go through membrane fusion and the virus is even known to induce cell–cell fusion (Herschhorn et al. 2011). Configurational changes of gp41 protein drive this membrane fusion. Thereby, the structure and function of the protein are well studied in the literature (Chan et al. 1997; Tran et al. 2012; Mao et al. 2013). For example, Mao et al. (2013), Tran et al. (2012), and Merk and Subramaniam (2013) have resolved the configurations of gp41 upon cryo-EM imaging of the protein at unliganded and liganded states. These configurations are in agreement with the earlier resolved crystallography structure of the protein (Chan et al. 1997; Weissenhorn et al. 1997; Caillat et al. 2021). The trimeric gp41 is of size $97 \times 101 \times 234$ $Å^3$ (Caillat et al. 2021). Each gp41 monomer consists of three major domains: an N-terminal ectodomain, a transmembrane domain (TMD), and a C-terminal cytoplasmic tail (CT) (Fig. 1A). The ectodomain has a fusion peptide (FP, residues 512–524), a fusion peptide proximal region (FPPR, residues 525–535), two hydrophobic heptad-repeat regions (HRs), i.e., HR1 (residues 536–594) and HR2 (residues 629–662), and a tryptophan-rich membrane-proximal external region (MPER, residues 663–682) (Caillat et al. 2021) (Fig. 3A). The overall structure of gp41 is dominated by α-helices (HRs and TMD) and loops (Fig. 3B). The FP and FPPR interact with the inner domain of gp120. In the trimeric protein, gp41 monomers associate through its TMD.

Complexation of HR1 and HR2 peptides results in the six-helical bundle configuration of gp41 which is the most characterized state of the protein (Chan et al. 1997; Weissenhorn et al. 1997). HR1 helices arrange internally as a parallel coiled-coil and HR2 helices orient externally in an anti-parallel manner in the complexed state (Fig. 3C). The antiparallel association of HR1 and HR2 forms an α-helical hairpin configuration which appears as a six-helical bundle in the trimeric gp41 (Fig. 3C and scheme in Fig. 4B-iv). This configuration appears at both pre-fusion (native or unliganded) and post-fusion states of Env (Fig. 4B-i and iv), although the HRs form shorter or broken helices in the pre-fusion state (Mao et al. 2013). The gp41 goes through multiple intermediates such as activated and pre-hairpin configuration during the transition from the pre- to post-fusion state. Cryo-ET studies by Tran et al. (2012) show that Env binding to either CD4 or 17b (a co-receptor mimic) leads to a less compact structure of HR1 helices within the six-helical bundle. The authors named it activated intermediate configuration. At the pre-hairpin configuration, the HRs form an extended metastable structure at which the internal HR1 helices become accessible for binding with complementary external peptides (enfuvirtide, a fusion inhibitor) (Kim and Chan 1998). Antiviral drug candidates can inhibit these configurational transitions of gp41 by stabilizing the

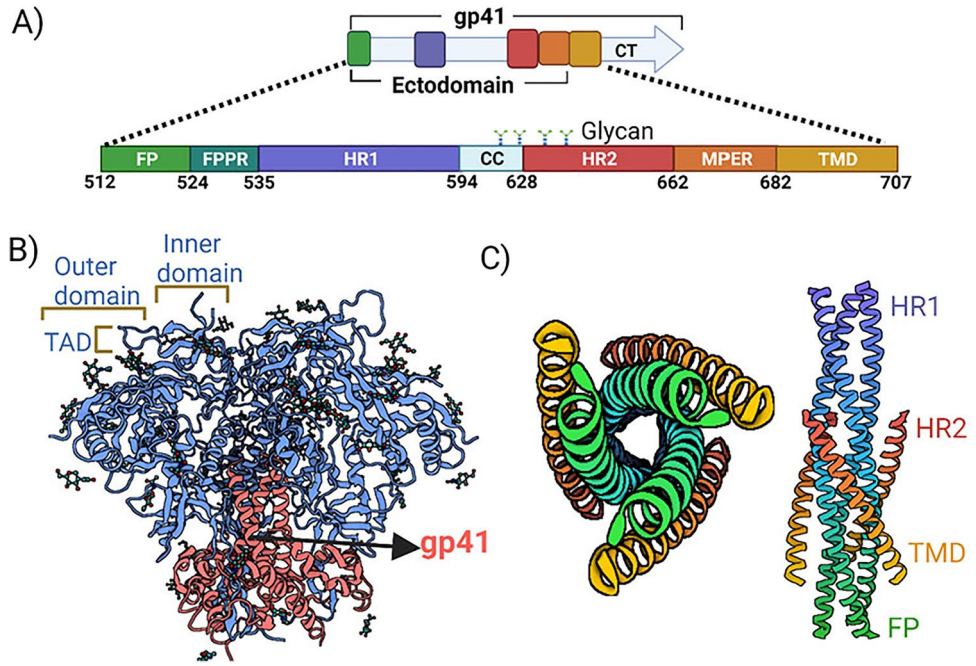


**Fig. 3** Structure of the gp41. **A** Diagram of the sequence and major domains of gp41. **B** Side view of the structure of trimeric Env. Here, the gp41 structure is visible as indicated by the dark orange color (PDB ID: 4ZMJ, pre-fusion structure). **C** Top (left) and side (right) views of the tertiary structure of gp41 at its post-fusion state (PDB ID: 1ENV, crystallography structure at 2.6 Å resolution (Weissenhorn et al. 1997). The FP and helices (HR1 and HR2) are shown according to the color coding of the protein sequence in (**A**). FP: fusion peptide; FPPR: fusion peptide proximal region; HR1: heptad repeat region 1; CC: Cys loop region; HR2: heptad repeat region 2; MPER: membrane proximal external region; TMD: transmembrane domain; CT: cytoplasmic tail. Created with Biorender.com

metastable pre-hairpin state or trapping the intermediate activated configuration.

**Cellular factors in the membrane attachment and fusion of HIV-1** The above-discussed configurational changes of gp41 cause major transformations in the enveloped state of the virus. Broadly, the steps that occur between the pre- to post-fusion of HIV-1 and other fusogenic viruses can be named as follows: virus docking/attachment, membrane tethering, membrane hemifusion (merging of apical membranes), and fusion pore opening (Fig. 4B-i to iv). Single-particle imaging techniques have been at the disposal to trace these steps at the single virus level (de la Vega et al. 2011; Ward et al. 2020) and also to find out molecular/cellular factors such as pH condition (Miyauchi et al. 2009), SERINC proteins (Ward et al. 2020), and lipid rafts (Simons and Ikonen 1997) associated with these steps.

Multiple groups have reported the influence of lipid order–disorder ($L_o$–$L_d$) domains on HIV-1 docking, hemifusion, and fusion (Yang et al. 2016, 2017). Yang et al. (2017) examined the effect of lipid domains by employing in vitro biomimetic platforms, in particular, giant plasma membrane vesicles (GPMVs) derived from host cells that express CD4 and CCR5 receptors. Like other transmembrane proteins, the membrane distribution of these receptors depends on $L_o$–$L_d$ domains or lipid rafts in cell membranes. Fluorescence images of GPMVs confirm that CD4 and CCR5 preferentially distribute in the $L_o$ phase and at the $L_o$–$L_d$ boundaries, respectively. Single-particle fluorescence imaging of HIV-1 Env particles (labeled with a membrane-anchoring fluorophore) shows that the viral particles prefer to attach to $L_o$–$L_d$ boundaries (Fig. 4B-i and micrographs in Fig. 4D), confirming that HIV-1 binds to both CD4 and CCR5 during the membrane attachment. Beyond the membrane attachment or docking of single HIV-1 particles, Yang et al. (2017) also detected fluorescence dequenching of the labeled virions. This occurs because of lipid mixing between the viral envelope and lipid bilayer of GPMVs. HIV-1 fusion inhibitors such as enfuvirtide lower the number of lipid-mixing events, confirming that the lipid-mixing phenomenon can be probed to evaluate the membrane hemifusion and fusion pore opening (Melikyan 2011). As HIV-1 particles dock preferably at the $L_o$–$L_d$ boundary, the respective lipid-mixing events are dominated at the phase boundary (Fig. 4B). Any disruption of $L_o$ domains such as cholesterol depletion causes a decrease in the lipid-mixing events and slows down the mixing kinetics. This indicates that the membrane receptor associated with $L_o$, i. e., CD4 is critical for the attachment as well as fusion of HIV-1.

To better understand the fusion steps, Yang et al. (2017) implemented the lipid-mixing assay using planar biomimetic systems, i.e., supported planar plasma membranes (SPPMs). Two major advantages of the planar platform over GPMVs are (1) the ability to detect multiple lipid-mixing events at a time, i.e., improved statistics, and (2) the determination of accurate lipid-mixing kinetics by using time-lapse total internal reflection fluorescence (TIRF) microscopy technique. With this setup, the authors could distinguish between the HIV-1 docking, hemifusion, and fusion pore opening steps (Fig. 4D, lower panel). They reported that more than 50% of the bound HIV-1 particles at the $L_o$–$L_d$ boundary fuse completely (fusion pore opening), whereas only 10% of the bound virions at $L_o$ domains fuse and the rest stays either at the docking or hemifusion state. $L_o$ domains or lipid rafts contribute to a higher line tension in membranes, and HIV-1 can have such domains or rafts in the viral envelope. The raft-rich envelope of HIV-1 may lower its line tension upon the membrane fusion at $L_o$–$L_d$ boundaries (Fig. 4B-iii and iv) (Yang et al. 2016). Thus, HIV-1 particles can preferentially bind to and fuse with domain boundaries on cell membranes. This could also explain the higher propensity of HIV-1 infection in activated $CD4^+$ T cells which are rich in lipid rafts (Janes et al. 1999; Yang et al. 2016).

Unlike the membrane factors that facilitate HIV-1 attachment and fusion, some cellular proteins act as viral restriction factors (Firrito et al. 2018). Transmembrane SERINC proteins are reported to have such activity (Sood et al. 2017; Chen et al. 2020; Ward et al. 2020). They can get incorporated in the envelope of HIV-1 (at *nef* deficient condition) during virus budding from the plasma membrane (Zhang et al. 2017). Ward et al. (2020) investigated the role of the SERINCs in the membrane attachment and fusion of HIV-1 particles using TIRF microscopy and cryo-ET. The authors observed that fluorescently labeled HIV-1 particles (pseudovirions, fluorescent proteins incorporated into the viral core via genetic engineering) attach to membranes for ~ 12 s followed by a relatively fast (within ~ 2 s) release of the viral internal content which confirms fusion pore opening. The kinetics of these steps do not alter for virus particles with SERINCs, but the number of fusion events decreases in the presence of either SERNIC3 or SERINC5. Complementary to the kinetics data, the authors traced the intermediate states between the docking and fusion of HIV-1 using single-particle cryo-ET. The corresponding images reveal that the number and types of the intermediate states are more for HIV-1 with either SERINC3 or SERINC5. The authors hypothesize that these two SERINCs increase the free energy barrier between the consecutive intermediate steps of HIV-1 fusion, lowering the chances of fusion pore formation or widening even after successful hemifusion (lipid mixing). Also, SERINCs are known to influence the distribution of lipids and proteins in cell membranes (Trautz et al. 2017). They may restrict the optimal distribution of Env (Chen et al. 2020) and/or reduce the lipid rafts in the viral envelope which in turn lowers the chances of fusion pore opening even after successful docking or hemifusion of HIV-1 particles.

**Fusion pathways of HIV-1 in host cells** Probing HIV-1 fusion on biomimetic membranes, like GPMVs and SPPMs, have provided information about the membrane processes at the single-virus level. A comprehensive understanding of HIV-1 fusion and its pathways can be attained if a similar set of experiments can be performed at the cellular level. For example, the lipid-mixing events of HIV-1 occur in a pH-independent manner both on model membranes (Yang et al. 2016) and cell membranes (Wilen et al. 2012). Interestingly, HIV-1 can also fuse in the acidic pH condition of endosomes and macropinosomes as observed in EM images of infected cells (Pauza and Price 1988; Maréchal et al. 2001). Other researchers also indicated that HIV-1 can take endosomal routes for virus entry and fusion (Fredericksen et al. 2002; Daecke et al. 2005; Miyauchi et al. 2009) (Fig. 4A).

In this context, Miyauchi et al. (2009) observed that membrane-impermeable fusion inhibitors did not block the membrane fusion of HIV-1 in host cells. The authors implemented time-lapse confocal imaging of dual-color HIV-1 in live infected cells and examined heterogeneity in the fusion pathways by tracking single virions. The authors designed fluorescence labeling of HIV-1 (pseudovirions) such that the virus envelope (tagged with a membrane-anchoring fluorophore) and inner content (NC tagged with a fluorescent protein) can be marked independently. In cases of fusion at the plasma membrane, the fluorescence signal from the marked viral envelope and inner content drops simultaneously because of their infinite dilution into the plasma membrane (via lipid mixing) and cytosol, respectively. This is not the case for endosomal fusion because the smaller surface area of endosomes does not result in infinite dispersion of the fluorescence signal upon the lipid mixing. Data of Miyauchi et al. indicates that HIV-1 takes the endosomal fusion pathway as they observed a considerable lag time between the lipid-mixing events and the release of virus internal content. Moreover, the viral content release is pH dependent whereas the lipid mixing is not. This means that HIV-1 particles can go through the membrane hemifusion step at the plasma membrane but the fusion pore opening occurs in the acidic endosomes (Fig. 4A). Similar dual-color imaging assays at the single virus level were implemented by Sood et al. (2016) and others (Campbell et al. 2007; Padilla-Parra et al. 2013; Coomer et al. 2020) for a better understanding of HIV-1 fusion pathways. Evidence suggests that fusion pore formation and its widening are energy-intensive steps and contribute to the overall energetics of the HIV-1 fusion process (Melikyan 2008). Since the HIV-1 fusion with the plasma membrane does not go beyond the lipid-mixing

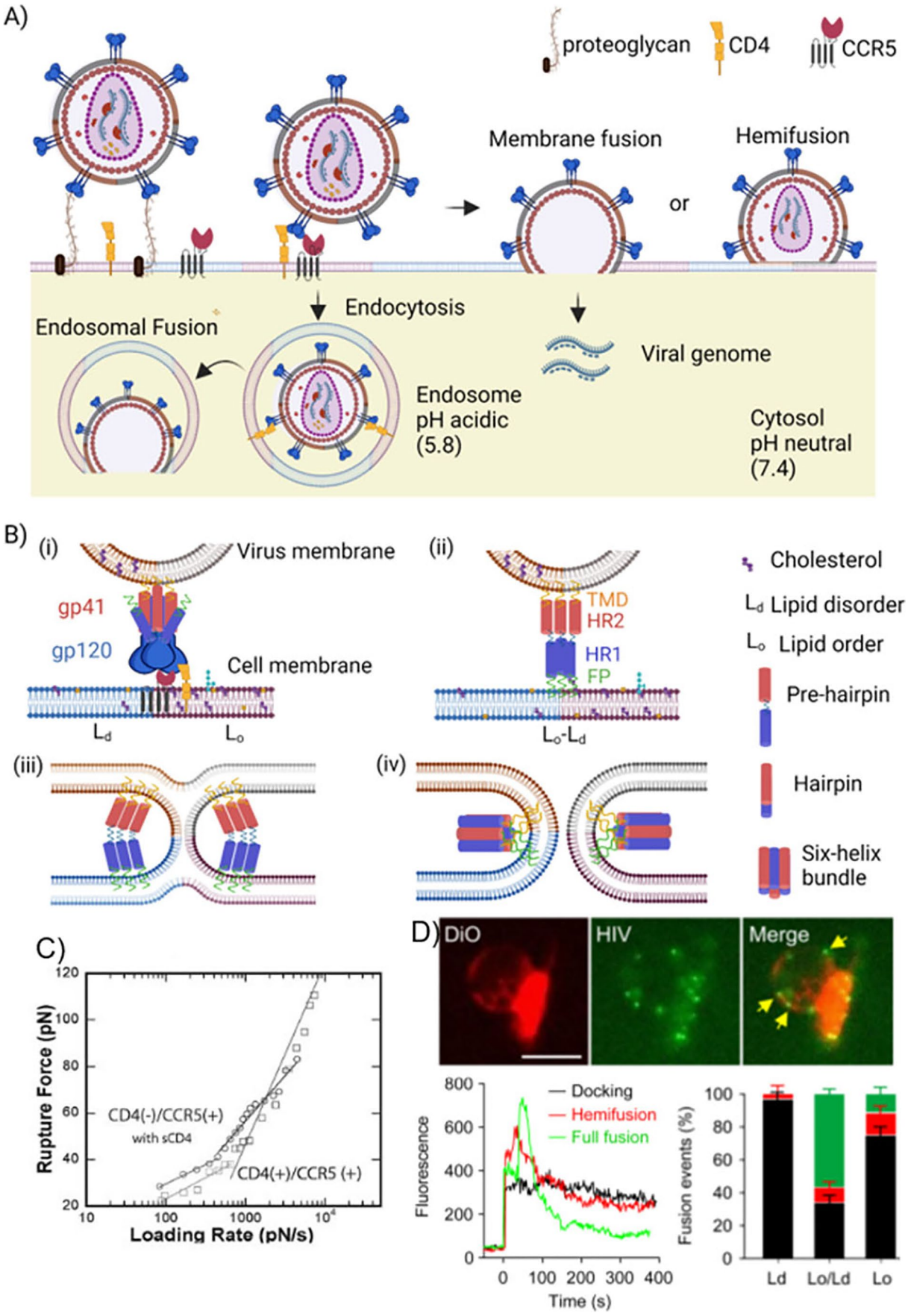
A)
proteoglycan
CD4
CCR5
Membrane fusion
Hemifusion
or
Endocytosis
Endosomal Fusion
Viral genome
Endosome
pH acidic
(5.8)
Cytosol
pH neutral
(7.4)
B)
(i)
Virus membrane
gp41
gp120
Cell membrane
Ld
Lo
(ii)
TMD
HR2
HR1
FP
Lo-Ld
(iii)
(iv)
Cholesterol
Ld Lipid disorder
Lo Lipid order
Pre-hairpin
Hairpin
Six-helix bundle
C)
Rupture Force (pN)
Loading Rate (pN/s)
CD4(-)/CCR5(+)
with sCD4
CD4(+)/CCR5 (+)
D)
DiO
HIV
Merge
Docking
Hemifusion
Full fusion
Fluorescence
Time (s)
Fusion events (%)
Ld
Lo/Ld
Lo

◂**Fig. 4** Membrane attachment and fusion of HIV-1. **A** Schemes depicting the attachment, hemifusion, and fusion of virions with a host cell. The virions interact with cell surface proteoglycans (HSPGs) and membrane receptors (CD4, CCR5). The virus fusion can take place either in a pH-dependent or pH-independent path. In the former path, bound virions are trafficked via endocytosis to acidic endosomes. The dual colors (dark red and gray; red and blue) on the viral envelope and cell membranes are to indicate the presence of lipid rafts or domains. **B** Schemes to illustrate the (*i*) interaction of the viral gp120 (at the pre-fusion state of Env) with CD4 and CCR5 which are distributed in $L_o$ and $L_o$–$L_d$ domains of a cell membrane, respectively. The membrane attachment of the virions is followed by (*ii*) membrane tethering, (*iii*) hemifusion, and (*iv*) fusion pore opening states. The pre-hairpin to hairpin transition of the gp41 leads to the membrane fusion of the virus. The hairpin structure appears as a six-helix bundle of the trimeric gp41. **C** Single-molecule force spectroscopy plot of gp120 interacting with receptors and co-receptors on the surface of GHOST Hi-5 cells. **D** Fluorescence micrographs showing the binding of labeled HIV-1 (in green) particles to GPMVs (in red). In the lower panel (left), temporal changes in fluorescence signal of the membrane-bound virus particle indicating the membrane docking, hemifusion, and fusion. The figure in the right lower panel shows the statistics of the events in $L_o$, $L_d$, and $L_o$–$L_d$ domains. (**A**) and (**B**) are created with Biorender.com. (**C**) is adapted with permission from Chang et al. (2005). Panels of (**D**) are adapted with permission from Yang et al. (2017)

step, targeting the fusion pore formation or widening in endosomes can better inhibit the virus fusion in host cells.

## Influenza A viruses

Influenza is an acute respiratory disease caused by the influenza viruses which belong to the *Orthomyxoviridae* family (Matrosovich et al. 2013). In 1918, the H1N1 strain of IAVs with genes of avian origin infected 500 million people and claimed an estimated 20 million lives worldwide. Due to their antigenic shift, subtypes of IAVs such as H1N1, H2N2, and H3N2 have caused multiple pandemics and a global death toll of about half a million per pandemic year. Although the majority of patients develop mild influenza disease with symptoms of common cold, about 5–10% of patients develop severe respiratory diseases, pneumonia, renal failure, and diabetes mellitus (Beumer et al. 2018). IAVs typically infect ciliated epithelial cells in the upper and lower respiratory tract of humans. Spike proteins of IAVs interact with cell surface glycans having terminal sialic acid (SIA) such as N-acetylneuraminic acid (Neu5Ac) and 9-O-acetyl-Neu5Ac. SIA is typically connected by glycosidic linkage to galactose (Gal). In humans, α-2,6 Neu5Ac is the primary attachment factor of the virus (Matrosovich et al. 2013).

IAVs isolated from hosts or cultured in the laboratory are of different sizes and shapes such as spherical with an average diameter of 120 nm, elongated up to an average length of 155 nm (Yamaguchi et al. 2008), and highly elongated or filamentous with a length that goes up to 500 nm (Vijayakrishnan et al. 2013). In general, each virion encloses eight segments of negative-sense RNA with 13,588 nucleotides that encode 11 proteins. Out of these, five are structural proteins, i.e., hemagglutinin (HA), neuraminidase (NA), M2 protein (proton channel), nucleocapsid protein (NP), and M1 protein (matrix protein) (Bouvier and Palese 2008). The former three together with a lipid bilayer form the envelope of the virus (Fig. 1B). The spike proteins, i.e., HA and NA, are the two major envelope proteins that drive the cellular attachment, fusion, and budding of IAVs (Fig. 1B) (Vijayakrishnan et al. 2013). A single influenza particle contains ~ 300–400 HA trimer and ~ 40–50 NA tetramer which protrudes out by about ~ 12.5–16 nm from the virus envelope (Harris et al. 2006). This relatively large number of spike proteins provides the "spiky" appearance of IAVs as observed in electron microscopy images (Harris et al. 2006; Shtyrya et al. 2009). The antigenic shift of IAVs comes from mutations/zootomic transitions that led to 18 HA and 11 NA subtypes which also gives the name of the virus subtypes H1N1, H2N3, etc. (Kosik and Yewdell 2019).

**Structure of HA and NA** Structures of the spike proteins of IAVs have been resolved using both X-ray diffraction and cryo-EM techniques with a resolution of 1.65 to 25 Å (Wilson et al. 1981; Harris et al. 2006, 2013; Fera et al. 2012). Harris et al. (2006, 2013) and Fera et al. (2012) solved the atomistic structure of HA on IAVs (H3N2, H1N1, and H2N2 strains) using cryo-EM. Their findings are similar to that of the previously calculated structures by Wilson et al. (1981) and Weis et al. (1990) from X-ray diffraction of the crystallized HA protein. These articles confirm that HA is a homotrimeric transmembrane glycoprotein with dimensions of ~ 135 Å (length) × 15–40 Å (radius) (Wilson et al. 1981). It has a threefold symmetrical axis and ~ 19 wt.% of the protein is glycosylated. Each monomer (M.W. of ~ 75–80 kDa) of the protein consists of two protein subunits, i.e., HA1 (328 aa) and HA2 (222 aa) (Wilson et al. 1981; Weis et al. 1990) (Fig. 5A, B). They are connected with a peptide bond (at Arg329) and one disulfide bond (cys14 of HA1-cys137 of HA2). The HA1 (35 × 45 Å) is the globular head of HA (Fig. 5B). It is mainly formed by eight stranded antiparallel β-sheets and the structure contains only 6% α-helix. Adjacent HA1 monomers make substantial contacts via their glycans. Interactions between the glycans and the hydrophilic amino acid residues (Ser and Thr) of the protein provide further stability to the trimeric head. HA1 connects to HA2 via two antiparallel helices. HA2 (~ 82 Å in length) is majorly constituted of α-helical coils that form the long stem of the spike protein (Fig. 5B). This subunit contains FP (residues 1–23; after 328aa of HA1), two heptad repeat regions, i.e., HR1 (residues 41–55) and HR2 (residues 77–101), transmembrane domain (TMD, residues 185–212), and cytosolic tail (CT, residues 213–222). The α-helices of HR1 and HR2 are

connected via a loop (residues 56–76), appearing as a hairpin structure (Fig. 5B-i). Three such hairpin helices packed together and twist ~ 100° around each other, appearing as six-helix bundles in the trimeric protein. The transmembrane part of HA2 is a 28 amino acid long helical chain, anchoring the trimeric protein in the viral envelope (Wilson et al. 1981).

Similarly, Fera et al. (2012) solved the atomistic structure of NA on IAVs (H2N2 strain) using EM technique. The structure is in agreement with one of the initial X-ray diffraction data of NA published by Varghese et al. (1983). The tetrameric transmembrane NA has a globular head ($95 \times 75 \times 77$ Å$^3$) and a stem that is 76 Å long. Each monomer of NA (M.W. of 60 kDa) consists of four distinct structural subunits, i.e., the catalytic head, the stalk/stem, the transmembrane region, and the cytoplasmic tail (Varghese and Colman 1991) (Fig. 1B). The enzymatic site is present in the catalytic head region which is formed by six identical antiparallel β-sheets and its active site consists of eight highly conserved functional charged and polar amino acids. The α-helical stalk connects the catalytic head and transmembrane region and also bridges two adjacent monomers by disulfide linkages (Varghese et al. 1983; Fera et al. 2012).

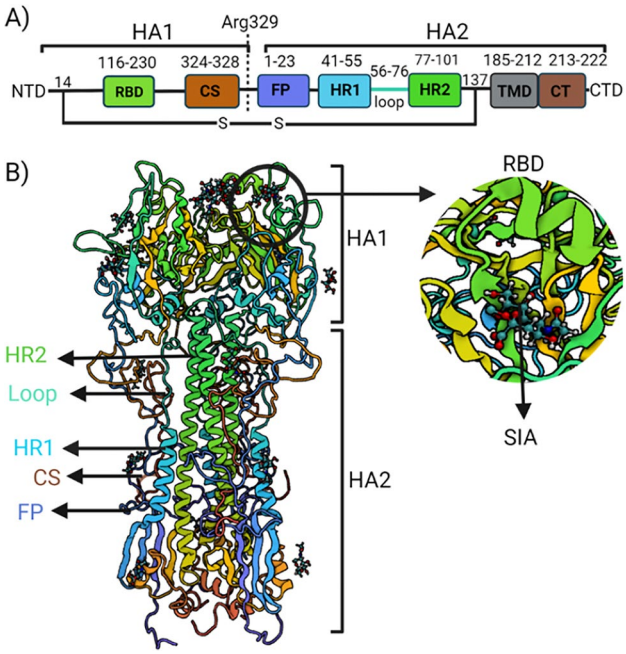


**Fig. 5** Structure of the HA protein. **A** Diagram of the sequence and major domains of HA showing the HA1 and HA2 subunits. **B** Side view of the structure of trimeric and prefusion HA protein (PDB-1HGE, X-ray diffraction structure at 2.6 Å resolution (Sauter et al. 1992). The RBD is encircled and other major domains are indicated with arrows. The color coding is according to (**A**). The encircled area is zoomed in to show the complexation of RBD with SIA. RBD: receptor binding domain; CS: cleavage site; FP: fusion peptide; HR: heptad repeat; TMD: transmembrane domain; CT: cytosolic tail. Created with Biorender.com

**Receptor binding site of HA and function of NA** The HA1 subunit contains the RBD (Fig. 5B). It engages in interactions with SIA forming a HA–SIA complex (zoom-in area of Fig. 5B) which has a relatively bent structure compared to the structure of free HA (Rogers and Paulson 1983). The binding site/pocket of RBD is resolved using both X-ray crystallography (Weis et al. 1988) and cryo-EM (Harris et al. 2013). Crystallography data of Weis et al. (1988), Skehel and Wiley (2000), Eisen et al. (1997), and Sauter et al. (1992) revealed that SIA binds to a shallow pocket of the RBD (Fig. 5B-ii). The edge of this binding pocket is constituted of three secondary structure elements (190-helix, 130-loop, and 220-loop) and its base contains multiple conserved residues which are the same for different IAV strains. The HA–SIA complex is formed via the following possible bonds: two H-bonds between the carboxylate group of SIA and HA's Ser-136 and Asn-137 residues; H-bond between the acetamido nitrogen of SIA and HA's Gly-135 residue; H-bond between 8-OH of SIA and HA's Tyr-98; four H-bonds between the 9-OH of SIA and HA's Tyr-98, His-183, Glu-190, and Ser-228 (Weise al. 1988). On the other hand, NA is a functional antagonist of HA. It catalyzes the hydrolysis of the glycosidic bond between SIA and galactose (Gal) in oligosaccharide chains (Byrd-Leotis et al. 2017). This way, it cleaves SIA from membrane receptors, contributing to the detachment of bound virions.

**Dynamic binding of IAV particles on the plasma membrane** The binding affinity ($k_D$) of a HA–SIA pair is not unique. The type of glycosidic linkage between SIA and consecutive saccharides in a glycoprotein/glycolipid receptor influences the affinity value. Fei et al. (2015) and Xiong et al. (2013) determined $k_D$ of 1–20 mM for HA–SIA pair by employing bioanalytical techniques like microscale thermophoresis and surface biolayer interferometry (BLI). The relatively high $k_D$ value (in the millimolar range) indicates that irrespective of multiple possible H-bonds between RBD and SIA, their molecular interaction is weak in the solubilized state. Hence, IAVs tend to form multiple HA–SIA pairs per virion for the membrane attachment. Because of this multivalent binding, HA–SIA pairs can rapidly form and break without causing complete detachment of the virus and providing temporary access to the viral NA for cleaving SIA from the membrane receptor (de Vries et al. 2020).

Besides the antagonistic functions of HA and NA, their distribution on the viral envelope is critical in regulating the dynamics of the virus attachment to cell membranes (Byrd-Leotis et al. 2017). Researchers using cryo-EM tomography have identified that the spike proteins form clusters such as an isolated NA surrounded by multiple HA (Harris et al. 2006; Matsuoka et al. 2009). We can say that the number of HA–SIA pairs per virion, enzymatic action of NA, and surface distribution of HA and NA control the

membrane-attachment dynamics of IAVs. Single-particle fluorescence imaging of IAVs (strain Aichi/2/68/H3N2) by Sakai et al. (2017) provided experimental proof of this hypothesis. The authors recorded the lateral movement of fluorescently labeled IAV particles bound on fetuin-coated surfaces using TIRF microscopy. Fetuin glycoprotein (FR) is rich in SIA and acts as a binding partner of the virus. Two-dimensional tracks of IAV particles reveal some exclusive features which are defined as crawling (speed < 0.2 μm/s) versus gliding (speed > 0.2 μm/s) motions (Fig. 6E). Both of the motions generate directional movement of IAVs on the FR surface and get blocked upon application of NA inhibitors or mutation (R103K) of NA's catalytic site. An exchange of HA–SIA pairs (breaking and making of HA–SIA pairs) occurs by the enzymatic activity of the viral NA (Fig. 6C, D), and that is why NA is essential for such directional mobility of the virions. In other words, multivalent interaction regulated by the antagonistic HA and NA results in the crawling and gliding motion of IAVs.

More recently, Müller et al. (2019) performed single-particle TIRF imaging to study the dynamics of IAVs binding on model membranes, in particular, receptor (GD1a) reconstituted supported lipid bilayers (SLBs). The authors determined kinetic parameters like attachment–detachment rate constant ($k_{on}$, $k_{off}$), residence time ($t_{res}$), and lateral diffusion coefficient ($D$) of SLB-bound virions. For this, they have implemented equilibrium fluctuation analysis (Gunnarsson et al. 2011) and single particle tracking (SPT). The authors observed that the $k_{on}$ and $t_{res}$ of IAV particles increase at higher receptor concentrations in SLBs. In accordance, the $k_{off}$ and $D$ of the bound particles decrease. This confirms the formation of multiple HA–SIA pairs per virion and the corresponding multivalency increases with increasing receptor availability. Although determination of the multivalency for such a dynamic system is not straightforward, the authors represented $\frac{1}{D}$ as the average valency or the average number of HA–SIA pairs per virion. The virus off-rate ($k_{off}$) versus this average valency shows a peculiar dependence, i.e., a decrease followed by a broad distribution, which means that the virus particles can detach from a membrane even after attaining a higher valency (Fig. 6D, F). This peculiarity appears because of the surface distribution (clustering) and antagonistic functions of HA and NA. At the higher valency of IAVs, the virus off-rate decreases but also the viral NA becomes more accessible to the bound SIA (Fig. 6D). The enzymatic action of NA contributes to the increased off-rate even when virions have lower mobility or greater valency. Blocking the NA's activity indeed eliminates such peculiar dependence and a continuous decrease of $k_{off}$ with increased $\frac{1}{D}$ (valency) can be observed.

Results of Sakai et al., Muller et al., and others show that the NA's activity is not limited to the budding of IAVs from cell membranes. The viral enzyme contributes to the dynamics of the virus attachment as well. Thus, the popular concept that NA inhibitors such as zanamivir and oseltamivir block the release of progeny IAVs may not be the only action mechanism of these drug molecules.

**Binding of IAVs to the cell surface glycans** While these biophysical studies confirm the multivalent binding of IAVs on SIA-rich biomimetic surfaces, it is essential to identify SIA-based membrane receptors and cell surface moieties which are actively involved in the cellular attachment and entry of the virions. Interestingly, the cell surface glycans which include glycolipids, glycoproteins, proteoglycans, and mucins are rich in SIA. Chu and Whittaker (2004), De Vries et al. (2012), and others (Mayr et al. 2018) reported the role of sialylated N-glycans in cellular infection caused by IAVs. Earlier, Chu and Whittaker (2004) employed fluorescence microscopy techniques to image the cellular attachment and endocytosis of IAV particles in CHO and Lec1 cells. The latter is deficient in sialylated N-glycans but has glycolipids and O-glycans. Irrespective of the virus attachment to both cell lines, the cellular entry or endocytosis did not occur in Lec1 which in turn lowered the infection level in the cell lines. The authors concluded that the sialylated N-glycans act as receptors for the cellular internalization of IAVs. Further cellular experiments by De Vries et al. (2012) show that IAVs can infect upon binding to O-glycans and glycolipids as well; however, the sialylated N-glycans become critical receptors in the presence of decoy SIA-glycans. This can be explained by the competitive binding of IAVs toward cell surface glycans and decoy agents. Possibly, the multivalent binding of IAVs toward N-glycans enables strong attachment and improved internalization of virions in host cells which is not the case for other glycans.

McAuley et al. (2017) reported that IAVs interact with cell-surface mucins which have O-glycans with terminal SIA, and the extracellular domain of mucins sheds upon the virus binding. This way, the cell-surface mucins act as releasable decoys, limiting the cellular attachment of IAVs (Fig. 6A). Recently, Honigfort et al. (2021) and Delaveris et al. (2020) synthesized mucin-mimetic glycopolymers for in vitro binding studies of IAVs. Their data indicates that the glycopolymers can either block the IAV binding or promote the retention of bound virions depending on the functional group and surface density of polymers (Fig. 6A, B).

Together, these data indicate that some of the native glycopolymers such as mucins and proteoglycans act as a protective steric layer or decoy agents against IAVs (Fig. 6A). Also, they can facilitate membrane attachment of the virions either by increasing the virus retention time or by guiding them such as via rolling motion (Fig. 6B) toward the plasma membrane. Hence, the distribution of cell-surface glycans and mucins can regulate the attachment–detachment of IAVs and may allow diversifying the hots cell tropism of the virus.

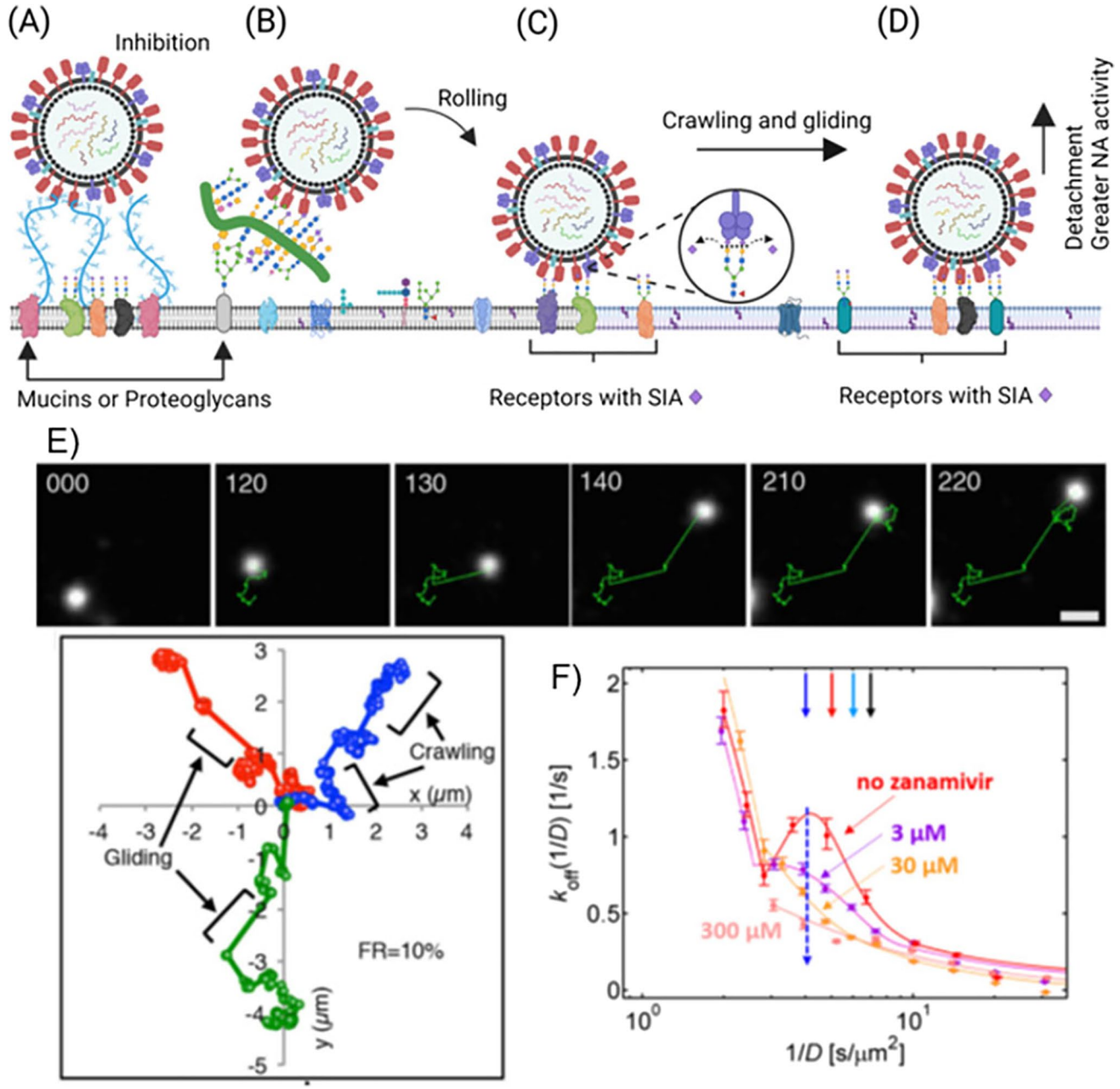


**Fig. 6** Schemes depicting the interaction of IAVs with cell-surface glycans and multivalent binding of the virions on the plasma membrane. (**A**) A virion is getting trapped by cell-surface mucins or proteoglycans. (**B**) A virion interacts with cell-surface mucins or proteoglycans. The particle can navigate through the surface glycans via its rolling motions and reach the plasma membrane. (**C**) Formation of multiple HA–SIA pairs per a single virion and the enzymatic activity of NA (zoom-in area) leading to the crawling and gliding motions of the particle. (**D**) A virion bound to the plasma membrane with a greater valency (more HA–SIA pairs per virion). An enhanced NA activity can lead to the detachment of the bound virion. (**E**) TIRF micrographs of a fluorescently labeled IAV particle at different timepoints. Tracks of three virus particles showing the gliding and crawling motions (lower panel). (**F**) Effect of a neuraminidase inhibitor on the plot of the off-rate of membrane-bound IAV particles versus the apparent average valency ($\frac{1}{D}$). (**A**)–(**D**) are created with Biorender.com. (**E**) and (**F**) are adapted with permission from Sakai et al. (2017) and Müller et al. (2019), respectively

**Configurational transitions of HA2** In host cells, membrane-bound IAVs get internalized via receptor-mediated endocytosis, trafficked through endosomes, and eventually fuse with the membrane of late endosomes (typically ~ pH 5, ranging from 4.6 to 6) (Scholtissek 1985; Zaraket et al. 2013). To initiate the fusion process, the HA protein goes through a priming process in which cellular enzymes such as serine proteases, transmembrane serine 2 or 4 (TMPRSS2 or

TMPRSS4), and human airway trypsin-like protease (HAT) (Klenk et al. 1975; Böttcher et al. 2006) cleave the peptide bond (at Arg329) (Wilson et al. 1981). This cleavage forms the C terminus of HA1 and the N terminus of HA2 which are separated by ~ 21 Å distance. At this state, the HA2 subunit can go through configurational changes that drive the viral fusion.

Multiple groups have resolved the structure of HA2 at neutral (pre-fusion) and acidic pH (fusion state) by using EM (Booy et al. 1985; Fera et al. 2012; Benton et al. 2020a) and X-ray crystallography (Wilson et al. 1981; Bullough et al. 1994). At the neutral pH, the hydrophobic FP (at the tip of HR1) is buried inside the pocket of HA2 six-helix bundles (Fig. 7A). A low pH condition triggers a loop-to-helix transition, i.e., the loop connecting the HRs converts into a helix and forms an extended coiled-coil HA2 (Fig. 7C). Cryo-EM images by Benton et al. (2020a) show that HA2 attains a 150-Å trimeric coil structure which is much longer compared to its length at the native/pre-fusion state, i.e., ~ 76 Å (Wilson et al. 1981). Also, the FP gets exposed to the globular head of HA (drawn in Fig. 7C). This is the pre-hairpin configuration of HA2 at which the FP becomes available to tether the viral envelope and the endosomal membrane (Fig. 7C, D-i). These changes alter the interactions between the HA monomers and their subunits, making the pre-hairpin configuration metastable. Benton et al. observed a displacement of the 30-loop (22–27 aa) of HA1 during native to pre-hairpin transition. It enables new interactions between HA1 and HA2 subunits, delaying the reverse transition to the native state and promoting an effective membrane tethering by the FP.

Next, a helix-to-loop transition at HR2 (residues 106–112) occurs. It causes folding of the extended coil (pre-hairpin) closer to the C-terminal side of HA2, forming a hairpin structure of the HA monomer and appearing as six-helix bundle for the trimer. The tethered membranes are pulled inwards and merge (fusion) during this structural folding (Fig. 7D). Overall, the HA2 protein transforms from the native hairpin to metastable pre-hairpin to post-fusion hairpin structure at acidic pH. These transformations occur via multiple intermediate configurations upon pH activation. Benton et al. (2020a), Das et al. (2018), Ni et al. (2014), and others employed time-dependent structural studies for resolving such configurations. Single-particle cryo-EM images of soluble HA show that the rotation of HA1 leads to the transient (10–20 s) dilated configurations

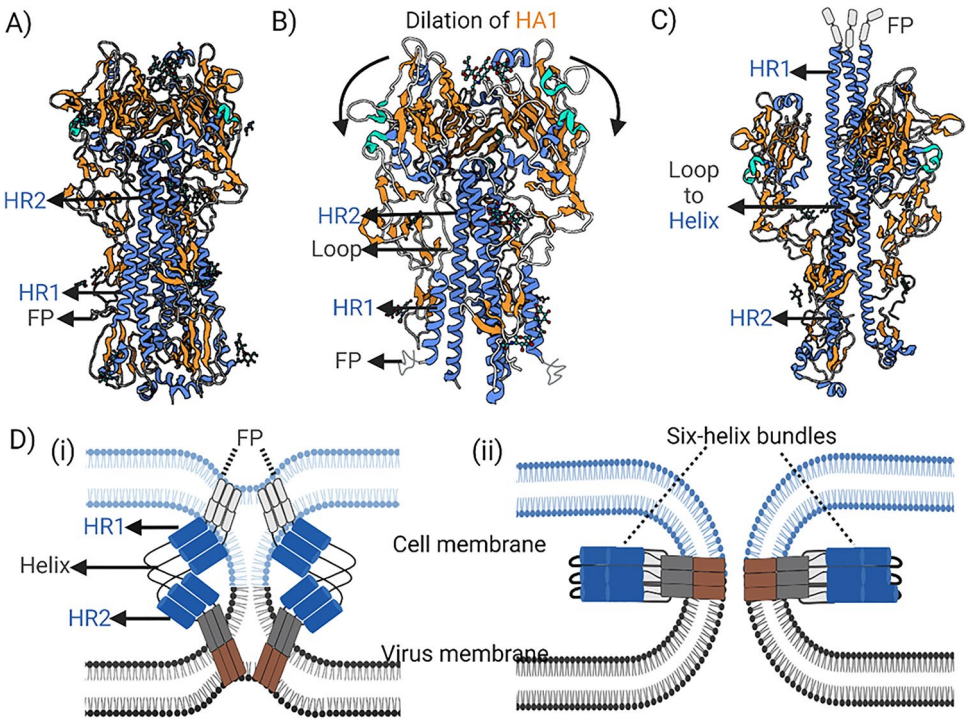


**Fig. 7** Configurational transitions of HA during the membrane fusion of IAVs. Side views of the structures of trimeric HA upon acidification (neutral to pH 5): **A** native pre-fusion (neutral pH), **B** intermediate dilated II (pH 5), and **C** extended or pre-hairpin (pH 5) conformation (cryo-EM structure with 2.6–5 Å resolution (Benton et al. 2020a) and the FP is drawn to indicate its position). The distance of HA1 monomers from the central axis increases upon transition from the native (35 Å) to dilated II (40 Å) to pre-hairpin (48 Å) configuration. Major domains of HA1 and HA2 are shown in orange and blue color, respectively. The FP and loop are shown in dark gray color. **D** Schemes showing the membrane (*i*) hemifusion and (*ii*) fusion pore opening process. The pre-hairpin to hairpin transition of HA results in the membrane fusion of the virus. The hairpin structure appears as a six-helix bundle for the trimeric HA. Created with Biorender.com

(Fig. 7B) at which HA1 domains tilt away from the central axis of the HA trimer and, consequently, the disordering of HA2 begins (Benton et al. 2020a). Das et al. (2018) detected three reversible configurations of HA at pH 7, i.e., pre-fusion (high-FRET), intermediate (moderate FRET), and coiled-coil/pre-hairpin (low FRET) using smFRET (by fluorescence labeling of 17 and 127 residues of HA2). While the percentage of the coiled-coil configuration increased at acidic pH, the configurational reversibility was maintained if the virions are exposed to an acidic condition for a limited time (5–15 min). Also, the binding of SIA to HA causes a shift toward the low-FRET configuration even at neutral pH. The SIA may have an allosteric effect, facilitating the release of the viral FP.

**Membrane fusion of IAV particles** Conformational changes of HA2 and their corresponding energetics drive the membrane fusion of IAVs. Membrane hemifusion and fusion pore opening have been imaged using electron and fluorescence microscopy techniques (Fig. 7D). Calder and Rosenthal (2016), Lee (2010), Fontana et al. (2012), and Gui et al. (2016) have imaged these fusion states employing cryo-ET technique. These studies confirm that majority of IAV particles (> 60%) are fully fused with artificial lipid membranes (liposomes) upon acidic treatment (pH 4.9) for 30 min. Calder et al. observed the formation of multiple contact zones between a single IAV and liposomes via multiple HA of ~ 18.5 nm length. This elongation of HA (~ 15 nm at the neutral pH) indicates the formation of pre-hairpin confirmation. Both Calder et al. and Lee et al. detected dimple contact points at which the target liposomal membrane is locally deformed (funnel shape) toward the virus. At these dimples, the viral envelope and target lipid membrane bridge via a 10–15-nm channel (Lee 2010) (hemifusion) and eventually form pores with a diameter of 14 ± 5 nm (Calder and Rosenthal 2016). Tomograms of the dimples show that the M1 protein of IAVs stabilizes the viral envelope during the membrane hemifusion. Fontana et al. (2012) show that at pH 4.9 (fully fused state), the M1 layer is dissolved in the majority of virions. The authors also observed disorganization of HA protein on the viral surface within 5 min of pH lowering and the changes were reversible within this timescale. The sub-tomogram analysis of the HAs on the viral surface revealed an intermediate configuration of HA at which the protein is a bit shorter in length (~ 13 nm) and wider (~ 7.5 nm) compared to its configuration at neutral pH (~ 15 × 6 nm).

While these structural studies provide the proof of the hemifusion and fusion pore formation states and associated HA conformations, the exact number of HA involved in the contact zones is difficult to be resolved. Early in 2008, Floyd et al. (2008) developed a fusion assay for probing the membrane fusion kinetics of IAVs and evaluating the number of HA involved per single fusion event. Similar assays have been applied by multiple researchers for analyzing the real-time kinetics of these membrane fusion states for IAVs (Costello et al. 2012, 2015; Ivanovic et al. 2013; Liu and Boxer 2020; Villamil Giraldo and Kasson 2020).

Floyd et al. (2008) imaged dual-color IAV particles bound to a biomimetic platform, i.e., receptor (GD1a) reconstituted SLBs on a thin dextran cushion and having a fluorescent pH sensor (fluorescein). The authors recorded fluorescence signals from the fluorescein, membrane-anchoring fluorophore tagging the viral envelope, and nucleotide-binding fluorophore tagging the viral genome. They represent the pH activation, lipid mixing, and fusion pore opening, respectively. The corresponding signals at the single-particle level confirm that the lipid mixing and fusion pore opening occurs within an average lag time of 15–20 s and 30–35 s from the pH activation, respectively. This lag-time data holds information about the rate-limiting steps involved in membrane hemifusion (lipid mixing) and fusion pore opening of single virions. Floyd et al. applied a kinetic model to calculate the number ($N$) of rate-limiting events from the corresponding lag-time distribution. According to this analysis, three rate-limiting events ($N_{min} \sim 3$) must occur for the hemifusion of IAVs, and hemifusion to fusion pore opening occurs in a single rate-limiting step. At the molecular level, the transition from hairpin to pre-hairpin configuration of HA2 is the rate-determining step of virus fusion. Thus, the calculated $N_{min} \sim 3$ corresponds to the minimum number of HA2 per virion going through this transition. In other words, the membrane hemifusion of IAVs proceeds via a set of parallel rate-determining configurational transitions with three participating HA, and subsequently the viral fusion (pore opening) occurs (Fig. 7D-i and ii). This data shows that synergistic or cooperative molecular/configurational transitions are essential for the successful membrane fusion of IAVs.

Ivanovic et al. (2013) and Costello et al. (2015) observed a similar synergistic or cooperative effect for the membrane hemifusion of different strains of IAVs (X-31, Udorn and Brisbane strains). Interestingly, the cooperativity of hemifusion as expressed with $N_{min}$ is the same (~ 3) irrespective of the type of virus strain and mutant, but the rate of hemifusion differs. Costello et al. (2015) reported that unlike the laboratory-adapted X-31 and Udorn strains, the Brisbane strain is more acid stable and has a fusion rate almost independent of acidic conditions (pH 5.5 to 4.5). Ivanovic et al. (2013) indicate that the release of the viral FP from sequestered pre-fusion structure becomes more facile in $G4S_{HA2}{}^{X31}$ and $D112A_{HA2}$ mutants. In the pre-fusion conformation of wild-type HA2, the Gly (G4) forms H-bonds with conserved aspartic acid (D112). A weakened H-bonding upon the mutations ($G4S_{HA2}{}^{X31}$ and $D112A_{HA2}$) lowers the kinetic barrier for the release of the fusion peptide. Together, these kinetic studies conclude that the criteria for membrane

hemifusion (lipid mixing) and fusion of a single virion are: (1) accessible and releasable FP in HA and (2) synergistic or cooperative configurational transitions of the HA protein.

**Membrane factors in IAV fusion** Lipid-mixing events are ubiquitous in cellular systems and a common example is lipid mixing during the release of neurotransmitters at synapses (Lu et al. 2005). Factors like lipid compositions, membrane rigidity, and membrane curvature are shown to affect such lipid mixing at synapses. The same membrane factors can also influence the lipid mixing during IAV fusion (Zhang et al. 2000; Liu and Boxer 2020; Villamil Giraldo and Kasson 2020). In this context, Villamil Giraldo and Kasson (2020) designed a biomimetic platform for probing the role of membrane factors in the virus. The authors compared the lipid mixing of fluorescently labeled IAVs (membrane-anchoring fluorophore) when bound to (1) hollow lipid vesicles which are deformable and (2) SLB on silica nanoparticles which are non-deformable. In general, the lipid-mixing kinetics is faster in the former. The authors evaluated the $N_{min}$ for the lipid mixing and described that it relates to the stochastic activation barrier for fusion. The $N_{min}$ for non-deformable SLB nanoparticles is higher compared and is also affected by changing their diameter (curvature). The authors concluded that the IAV fusion is regulated by the membrane deformation, and the curvature effect is associated with the membrane deformation. The rigidity or fluidity of a membrane determines its deformability which can influence the membrane mechanics, HA availability (in the viral envelope), and HA tethering, whereas the local membrane curvature can have a minimal effect because at the molecular or single virus level, the membrane may appear nearly flat.

A pertinent question is whether the membrane deformation and curvature have any physiological relevance to the fusion of IAVs in host cells. Recently, Haldar et al. (2020) examined this by probing the lipid mixing of IAVs (A/Aichi/68; H3N2) in endosomes that are isolated from infected host cells. Encapsulated virions in polydispersed endosomes are visualized in cryo-EM images. Colocalization imaging of fluorescently labeled IAVs and endosomal marker confirm that the virus particles are encapsulated in endosomes, and a rapid lipid mixing between them can be detected only at acidic pH. Also, the primary phase of the lipid-mixing kinetics is similar in both the endosomal membrane (negative curvature) and SLB-nanoparticle systems (positive curvature) (Villamil Giraldo and Kasson 2020), confirming that the membrane curvature has no direct role in IAV fusion. The authors reported that interferon-induced transmembrane (IFITM3) protein can regulate the deformability of endosomal membranes. The protein is reported as a cellular restriction factor for IAVs, although it is majorly distributed on the apical side of endosomal membranes and cannot be in direct contact with HA or other surface proteins of the virus (Li et al. 2013; Desai et al. 2014). The restriction mechanism of IFITM3 may work by reducing the deformability (fluidity) of endosomal membranes which in turn increases the fusion energetics.

## Severe acute respiratory syndrome-related coronavirus 2

Coronavirus disease 2019 (COVID-19) is an ongoing pandemic that is caused by SARS-CoV-2. In December 2019, the virus was first identified in Wuhan (China). Since then, it has rapidly spread across the continents. A majority of the COVID patients developed mild disease with symptoms of fever, cough, fatigue, and loss of taste and smell (Harrison et al. 2020; Mason 2020). However, 10–15% of the patients developed severe diseases developing hypoxia, mild to severe pneumonia, and lymphopenia. Because of the absence of specific therapeutics and the high transmission rate of the virus, the disease has taken a toll on public health by infecting more than 330 million people and claiming more than 5.55 million lives worldwide. The disease pathogenesis confirms that SARS-CoV-2 primarily infects the upper and lower respiratory tract (URT and LRT), causing acute respiratory disease (Hou et al. 2020). In particular, ciliated and olfactory epithelial cells in the URT and type II alveolar epithelial cells in the LRT get infected by the virus (Ahn et al. 2021; Mulay et al. 2021).

SARS-CoV-2 is a positive-sense single-RNA virus and a member of the beta coronavirus genus. It has one of the largest viral genomes, i.e., 29,881 nt, which encode 9860 amino acids (Wu et al. 2020). These amino acids form four structural proteins, i.e., spike (S), membrane (M), envelope (E), and nucleocapsid (N). The S, M, and E transmembrane proteins together with a lipid bilayer form the envelope of the virus (Fig. 1C). The N proteins remain associated with RNA creating a nucleocapsid inside the envelope and have vital functions in the late-phase replication of the virus such as assembly and budding. Among the envelope proteins, the S protein is the largest in size and is widely studied. It protrudes out by ~ 10–15 nm from the virus envelope (Ke et al. 2020; Klein et al. 2020), giving the virus a crown-like appearance. EM images of the virus indicate that the surface density of S protein is ~ 25–50 which is higher than the Env density of HIV-1 (Ke et al. 2020; Klein et al. 2020). Because of the surface representation and availability, the S protein is a major viral protein that interacts with cell surface receptors and its different epitopes are targets of antibodies produced by the human immune system. Hence, the S protein has been a prominent target for the development of antiviral drugs (Huang et al. 2020; Liu and Yang 2021). Also, it is a prime antigen for designing vaccine candidates (Kyriakidis et al. 2021).

**Structure and conformational dynamics of the S protein** The spike protein of SARS-CoV-2 is critical for the receptor recognition, membrane attachment, and fusion of the virus (Walls et al. 2016, 2020; Shang et al. 2020b; Wrapp et al. 2020). It is a homo-trimeric glycoprotein formed upon H-bond interaction between the adjacent S monomers (Kalathiya et al. 2020). Each monomer of the S protein (M.W. of 180–200 kDa) is made of 1273 amino acids (Fig. 8A) and has ~ 22 N-glycosylated sites (Watanabe et al. 2020). It is cleaved into two subunits S1 and S2 by host furin protease but remains non-covalently bound in its prefusion conformation (Walls et al. 2020; Wrapp et al. 2020; Tang et al. 2021). The S1 structure is composed of N-glycosylated β-sheets and appears like bulbous heads of the trimeric S protein (Figs. 1C and 8B). The N-terminal domain (NTD, residues 14–306) and receptor binding domain (RBD, residues 331–528) of the S1 monomer are at the apex (Fig. 8B, C). They are connected via a loop. The bottom side which is also the C terminus side of the S1 protein has two subdomains (SDs), i.e., SD-1 and SD-2 (Fig. 8C). They have major contact areas with the S2 subunit and also contain a furin cleavage site. From the top view of the S protein, it is clear that the NTD is oriented outwards of the S1 and the RBD is located closer to the threefold symmetry axis of the trimeric S protein (Fig. 8B, D).

The structural dynamics of the S1 subunit, in particular, the dynamic positions of the RBD, are well captured by the cryo-EM technique. Wrapp et al. (2020) and Walls et al. (2020) identified major conformations of the S protein in the early time of the COVID-19 pandemic. They resolved the structures upon a 3D reconstruction of cryo-EM images of the protein at its prefusion state. Two major structures of the protein are open and close conformations. In the open conformation, one RBD of the trimeric protein flanks upwards whereas the other two RBDs remain in their original position (denoted as "down"). These "up" and "down" positions of RBDs can be seen both in the side and top view of the trimeric S protein (Fig. 8C, E). In the close conformation, the inside cavity of the protein is stabilized by the interdomain contacts such as RBD-RBD, RBD-NTD, and H-bonds between N-glycans and RBD. Loss of these interactions leads to the transition from the "down" to "up" position

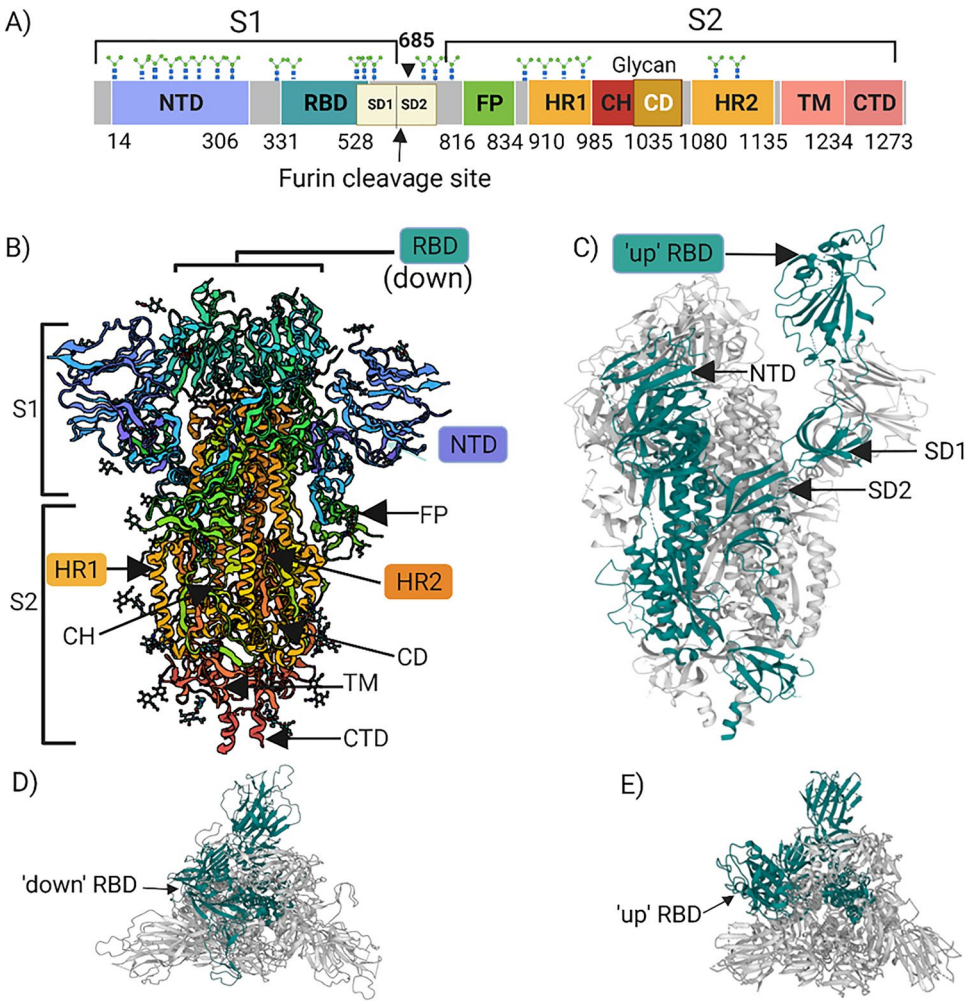


**Fig. 8** Conformations of the S protein of SARS-CoV-2. **A** Diagram of the sequence and major domains of the S protein showing the S1 and S2 subunits. Side view of the structures of the trimeric and prefusion S protein at **B** the close conformation (PDB ID: 6VXX, cryo-EM structure at 2.8 Å resolution (Walls et al. 2020) and **C** open conformation (PDB ID: 6VYB, cryo-EM structure at 3.2 Å resolution). The sub-domains in (**B**) are indicated with arrows and according to the color coding of (**A**). One RBD at the "up" position, NTD, and SDs are indicated by arrows in (**C**) (one of the S monomers is shown in green color). Top view of the structures of the trimeric and prefusion S protein at the **D** close (PDB ID: 6VXX) and **E** open conformation with one "up" RBD (PDB ID: 6VYB). RBD: receptor binding domain; NTD: N-terminal domain; SD: subdomain; FP: fusion peptide; HRs: heptad repeats; CH: central helix; CD: connecting domain; TM (or TMD): transmembrane domain; CTD: C-terminal domain (or CT: cytoplasmic tail). Created with Biorender.com

of an RBD resulting in the transition from the close to open conformation, and it occurs via at least two intermediate configurations (Mori et al. 2021). The extent of the conformational dynamics determines the equilibrium structure of the S protein (Lu et al. 2020). The "up" RBD is more accessible for binding to membrane receptors (Walls et al. 2020; Wrapp et al. 2020).

Beyond these structural analyses of the soluble S protein, Ke et al. (2020) resolved the structure and surface distribution of the S protein on intact virions using cryo-ET. The S protein is predominately at the prefusion state on the viral envelope, and the majority (81%) of the S monomers contain the "down" RBD. The refined structures even show the conformation of the S trimer on a single virion. About 53% and 47% of the S trimer on the viral envelope is in the closed and open conformation, respectively (Ke et al. 2020).

**Receptor binding site of the S protein** It is well established that the angiotensin-converting enzyme 2 (ACE2) is a cellular receptor of SARS-CoV-2 (Shang et al. 2020a; Zhou et al. 2020) (Figs. 9A and 10A). It is abundant in human tissues and expressed on type II alveolar epithelial cells in the lungs or LRT (Hou et al. 2020). Lan et al. (2020) and Shang et al. (2020b) resolved the crystal structure and interaction sites of the RBD–ACE2 complex with a resolution of ~ 2.5 Å. Both studies show that a receptor binding motif (RBM, 438–506 aa) of the RBD interacts with the N-terminal helix of ACE2 within a cut-off distance of ~ 4 Å (Fig. 9C). Lan et al. (2020) reported that about 17 amino acid residues of the RBM are in contact with about 20 amino acid residues of ACE2, whereas Shang et al. (2020b) concluded that about nine residues in the RBM are critical for the ACE2 binding. These studies also compared the structure of RBM–ACE2 complex of SARS-CoV-2 with that of SARS-CoV. There is a subtle difference in the RBM sequence of the two viruses and the respective RBM–ACE2 interaction sites. Interestingly, both RBMs interact with ACE2 via 13 H-bonds and 2–3 salt bridges (Lan et al. 2020). Shang et al. mentioned the formation of an additional H-bond in the RBM–ACE2 interface for SARS-CoV-2, causing its RBM to attain better or more compact contact with the ACE2 helix. The authors also reported that salt bridges of SARS-CoV RBM–ACE2 complex are relatively weaker.

Lu et al. (2020) implemented smFRET upon labeling specific sites before and after RBM (Q3 at RBD and A4 at SD1) of the S protein embedded on intact virions (chimeric and virus-like particles). The authors reported four reversible and dynamic conformations among which an intermediate FRET of ~ 0.5 represents the close conformation with three "down" RBDs. The ACE2-binding shifts it to a "fully" open conformation with three "up" RBDs (FRET of ~ 0.1). The authors detected that this shift is continuous (via intermediate conformations) and pronounced upon the binding with dimeric ACE2 compared to ACE2 monomer. A similar "fully" open conformation of the S protein has been detected upon cryo-EM imaging (Benton et al. 2020b; Henderson et al. 2020). The resolved structures by Benton et al. (2020b) show that a majority (~ 50%) of the ACE2-bound S protein has one "up" RBD and a sizable population has two or three "up" RBDs.

**Binding affinity of the S protein to the membrane receptor** Beyond the structural characterizations, biophysical techniques like SPR and BLI have been integral in the COVID-19 research. These tools have been applied for evaluating the binding affinity ($k_D$) of ACE2 toward the RBD of SARS-CoV-2 and also other coronaviruses like SARS-CoV and MERS. Lui et al. (2020) concluded that the RBD of SARS-CoV-2 interacts with dimeric ACE2 with limited intra-spike avidity. They determined the avidity by comparing the binding affinity of RBD as well as the S trimer toward monomeric and dimeric ACE2 by employing BLI technique. The binding affinity increases by ~ 1000-fold from monomeric to dimeric ACE2, confirming the binding avidity of the S protein. Wrapp et al. (2020), Walls et al. (2020), and others (Lui et al. 2020; Shang et al. 2020b; Wang et al. 2020; Zhu et al. 2021) implemented SPR or BLI technique to follow the association–dissociation kinetics of soluble dimeric ACE2 protein to surface-immobilized S protein. From these experiments, Wrapp et al. evaluated a $k_D$ value of ~ 15 nM for the ACE2-S protein pair and a similar $k_D$ (34.6 nM) value was obtained for truncated S1 protein that has one RBD. The protein–protein interaction results in this high binding affinity (low $k_D$). These solution-phase binding data confirms that only one RBD of the trimeric S protein interacts with dimeric ACE2 with the most optimal avidity. In agreement with the structural studies, we can say that it is the "up" RBD in the open conformation of the protein (Fig. 9B).

The high structural similarity between the RBM–ACE2 complex of SARS-CoV-2 and SARS-CoV has led researchers to compare the binding affinity of their S protein toward the ACE2 receptor (Li 2016; Lan et al. 2020; Shang et al. 2020b; Walls et al. 2020; Wrapp et al. 2020; Dutta et al. 2022). Multiple studies reported or mentioned that the receptor-binding affinity is higher for SARS-CoV-2 (Andersen et al. 2020; Shang et al. 2020b; Wrapp et al. 2020). The $k_D$ determined by Wrapp et al. (2020), Lan et al. (2020), and Shang et al. (2020b) employing the SPR technique ranges between 5 and 40 nM (Fig. 9D). The reasons for this variability in $k_D$ value can be the difference in the protein sequence and the binding model used for the analysis. A common feature reported in these works is that the $k_D$ is ~ 10 to 20 times lower for SARS-CoV-2 compared to that of SARS-CoV. Shang et al. explained that this increased affinity is because of the compact structure and stronger binding (H-bond and hydrophobic interaction) of the RBM–ACE2

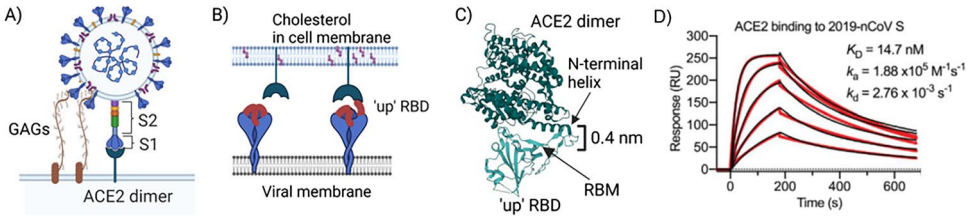


**Fig. 9** Receptors and attachment factors involved in the membrane attachment of SARS-CoV-2. **A** Schematic of a virion interacting with cell surface GAGs and ACE2 dimer which are the attachment factor and membrane receptor of the virus, respectively. **B** Scheme showing the "up" RBD of the S protein and its interaction with the dimeric ACE2 in a cell membrane rich in cholesterol. Membrane cholesterol can affect the ACE2 distribution and, thereby, the distribution of bound virions on the plasma membrane. **C** Structure of the "up" RBD complexed with human ACE2 dimer (PDB ID: 6vw1, X-ray crystallography structure at 2.68 Å resolution (Lan et al. 2020; Shang et al. 2020b)). RBM: receptor binding motif. **D** SPR binding traces of ACE2 to the surface-functionalized S protein of SARS-CoV-2. (**A**)–(**C**) are created with Biorender.com. (**D**) is adapted with permission from Wrapp et al. (2020)

pair. Another reason can be the lower glycosylation of the S protein in SARS-CoV-2, causing a better availability of the receptor-binding sites (Casalino et al. 2020; Watanabe et al. 2020). Contrary to these data, Walls et al. (2020) reported a similar affinity of the S proteins ($k_D$ ~ 1.2 to 5 nM) for both coronaviruses and explained based on the identical 14 amino residues in the RBM of their S proteins. In another paper, Shang et al. (2020a) employed a protein pull-down assay to compare ACE2-binding affinity for the two coronaviruses. The authors reported that while the RBD of SARS-CoV-2 has a higher affinity, the full-length S protein of the virus has a lower affinity. The application of different methodologies for the S protein expression and techniques for binding experiments might be the reason for the observed differences in the binding affinity. Irrespective of this, it is well accepted that the S protein of both coronaviruses has structural symmetry, common interaction sites, and nanomolar $k_D$ (high receptor affinity).

The binding of SARS-CoV-2 particles to ACE2 in the plasma membrane is likely to have more complex features, and the membrane attachment of virions may not be solely explained by the solution phase affinity or avidity of the S protein. Factors like conformational dynamics of the S protein (Wrapp et al. 2020; Mori et al. 2021), distribution of ACE2 in the plasma membrane (Zang et al. 2020; Sanders et al. 2021), and their cooperative or multivalent interaction (Pak et al. 2022) contribute to the overall attachment of the virus. These processes and interactions can be resolved if the binding is probed on host cells and at single virus level.

In this context, Yang et al. (2020) investigated the binding of ACE2 and the S protein at the single-molecule level using biomimetic platforms and model host cells. The authors employed force microscopy and functionalized AFM tips with either the S1 subunit or RBD such that the receptor-binding site is accessible. The force curves are traced by approach–reproach of the functionalized AFM tip to either ACE2-grafted surfaces or live A549 cells expressing ACE2 in the plasma membrane. The measured force curves and the corresponding binding probability confirm the binding specificity of the RBD toward dimeric ACE2. The force maps on live cells show that the adhesion force of the protein is much higher (~ 1.5 times) on cells expressing ACE2. The lifetime ($\tau$) of the S1–ACE2 pairs is ~ 125 ms which corresponds to $k_D$ (from the binding probability) of ~ 120 nM. This nanomolar $k_D$ of spike protein confirms a high affinity of the protein, although the value is higher than the $k_D$ values reported by Wrapp et al. (2020) and Walls et al. (2020) using soluble proteins. In addition, the force map generated in the AFM measurements indicates that the S1–ACE2 or RBD–ACE2 pair attain the bound state when separated by a distance of ~ 0.8 nm which is in a similar range as evaluated from the structural studies (Lan et al. 2020) (Fig. 9C). These data of Yang et al. confirm that membrane ACE2 is indeed a binding partner of the S protein and a cellular receptor of SARS-CoV-2 (Figs. 9A and 10A).

So far, similar binding experiments at the single virus level are yet not reported. Recent coarse-grained modeling by Pak et al. looked into the SARS-CoV-2 binding at the interface of the viral envelope and ACE2-rich membrane (Pak et al. 2022). The simulation data show that a single S trimer can bind to multiple ACE2 and the S protein attains more than one "up" RBDs during such binding. Interestingly, this multivalent binding leads to the dissociation of the S1 subunit from the S protein. This dissociation is enhanced with increased ACE2 per S protein at the interface, indicating a cooperative binding of the spike to the membrane ACE2.

**Binding of the S protein to the cell surface glycans** The pathogenesis of severe COVID-19 patients confirms that SARS-CoV-2 causes a high rate of cellular infection in the lungs (LRT) (Hou et al. 2020; Mulay et al. 2021). However, ACE2 is not that highly expressed in the LRT, and organs like the small intestine and kidney are rich in ACE2 (Hamming et al. 2004). This indicates that the virus is likely to use other membrane receptors, co-receptors, and attachment

factors for their attachment to and fusion with host cell membranes. Multiple groups have reported that cell surface glycosaminoglycans (GAGs) such as heparan sulfate (HS) and heparin (HP) act as attachment factors of the virus (Clausen et al. 2020; Kim et al. 2020; Mycroft-West et al. 2020; Tandon et al. 2021) (Fig. 9A). HS and HP are highly sulfated GAGs (~30% and 60–80% sulfation) and generate a high surface negative charge. The RBD contains a gathering of positively charged amino acids (Clausen et al. 2020; Kim et al. 2020), making it suitable for electrostatic interactions with the sulfated GAGs. Kim et al. (2020) resolved the molecular interactions between the S protein and GAGs using computation docking analysis and even determined the binding affinity ($k_D$) from the respective binding kinetics measured using the SPR technique. Their docking data show that the S protein contains three GAG-binding sites, i.e., 453–459 aa (YRLFRKS) within RBD, 681–686 aa (PRRARS) at the furin cleavage site of S1/S2, and 810–816 aa (SKPSKRS) of S2. The protein shows a greater affinity toward more sulfated GAGs. Its $k_D$ toward HP (highest degree of sulfation) is ~50 pM, which is comparable to the $k_D$ of ACE2-S protein. Ionic interactions between negatively charged sulfate groups on GAGs and positively charged lysine/arginine-rich residues of the S protein contribute to this high affinity (Yu et al. 2021).

Cryo-EM studies by Clausen et al. (2020) show a similar finding that HS and HP bind to the S protein and the binding site is close to that of the ACE2 binding site. At the cellular level, the binding of S protein to the GAGs influences the conformational dynamics of RBD, favoring the open conformation of the protein. The authors came to this conclusion from the S protein binding to host cells (A549, A375) expressing either ACE2 or HS or both. Their flow cytometry data shows that the binding of the viral protein to ACE2 increases by four folds in the presence of HS. This means that HS acts as a co-receptor or attachment factor of the virus (Clausen et al. 2020) (Figs. 9A and 10A). Therefore, the membrane attachment of SARS-CoV-2 is not limited by the binding affinity/avidity toward ACE2 and cell surface factors like GAGs promote the receptor binding or involve in cooperative interaction. This is a potential contributing factor to the increased cellular transmission of SARS-CoV-2 (Kielian 2020) and may even regulate the cell tropism of the virus (Chu et al. 2020).

**Structure and configurational transitions of the S2 subunit** Fusion of SARS-CoV-2 with a cell membrane is driven by configurational changes of the S2 subunit of the S protein. The subunit becomes accessible and gains confirmational activity upon the proteolytic cleavage of the S protein (Fig. 10B). Wrapp et al. (2020), Walls et al. (2020), and others (Cai et al. 2020; Ke et al. 2020) reported the 3D structure of the trimeric S2 subunit at its prefusion state with a resolution of ~3 Å. The major structural components of the protein according to these studies are fusion peptide (FP, residues 817–834), heptad region 1 (HR1, residues 911–985), central helix (CH, residues 987–1034), connector domain (CD, residues 1080–1135), heptad region 2 (HR2, residues 1163–1210), transmembrane domain (TM, residues 1214–1234), and C-terminal domain (CTD, residues 1235–1273) (see Fig. 8A and B). The helical TM domain anchors the S2 in the viral envelope. In particular, the FP is a short segment of 15–40 amino acids at the tip of the S2 protein. It is rich in hydrophobic residues, such as glycine (G) or alanine (A). The reason for its variable length is the difference in the designation of the viral FP by different research groups. The α-helical HR1 and HR2 are composed of repetitive heptapeptide, HPPHCPC, where H represents a hydrophobic or bulky amino acid residue, P is a polar or hydrophilic residue, and C is a charged residue.

Major configurational changes of the FP, CD, and HR domains determine the pre-fusion and post-fusion state of the S2 protein (Casalino et al. 2020) (Figs. 8B and 10C). The binding of the S1 subunit to ACE2 followed by an enzymatic activation of the S2 subunit triggers these configurational changes. However, it has been challenging to experimentally resolve the structural dynamics of the S2 protein. Molecular dynamics (MD) simulations have been a powerful tool in identifying the intermediate configurations between the pre- and post-fusion states of the protein and thereby tracing its configurational dynamics (Casalino et al. 2020; Roy et al. 2020; Dodero-Rojas et al. 2021). In particular, Casalino et al. (2020) and Dodero-Rojas et al. (2021) implemented an all-atom structure-based model of the S protein and performed MD simulations. The S1 and HR2 are the most glycosylated parts of the protein (Cai et al. 2020). Casalino et al. observed that the N-glycans of the S1, in particular, N165 and N234 glycans of its NTD, stabilize the "up" RBD, promoting the open conformation that essentially engages in the receptor binding.

Dodero-Rojas et al. (2021) also reported that the glycans of the S protein facilitate the membrane recruitment and fusion of SARS-CoV-2. The authors observed that the bulky glycans cause a transient caging of the HR1, CH, and CD domains of the S protein. The HR1 can be better directed toward the cell membrane and the probability of the FP crossing the cell membrane increases because of this caging effect. In the absence of the glycans, only one or two FPs of the S2 trimer can reach the cell membrane and fails to capture the host cell (Dodero-Rojas et al. 2021). Insertion of three FPs results in successful tethering between the viral envelope and host cell membrane (Fig. 10D-i). This is the metastable pre-hairpin state of the S2 protein at which the HRs are at extended helical. Favorable interactions between the H residues of HRs drive

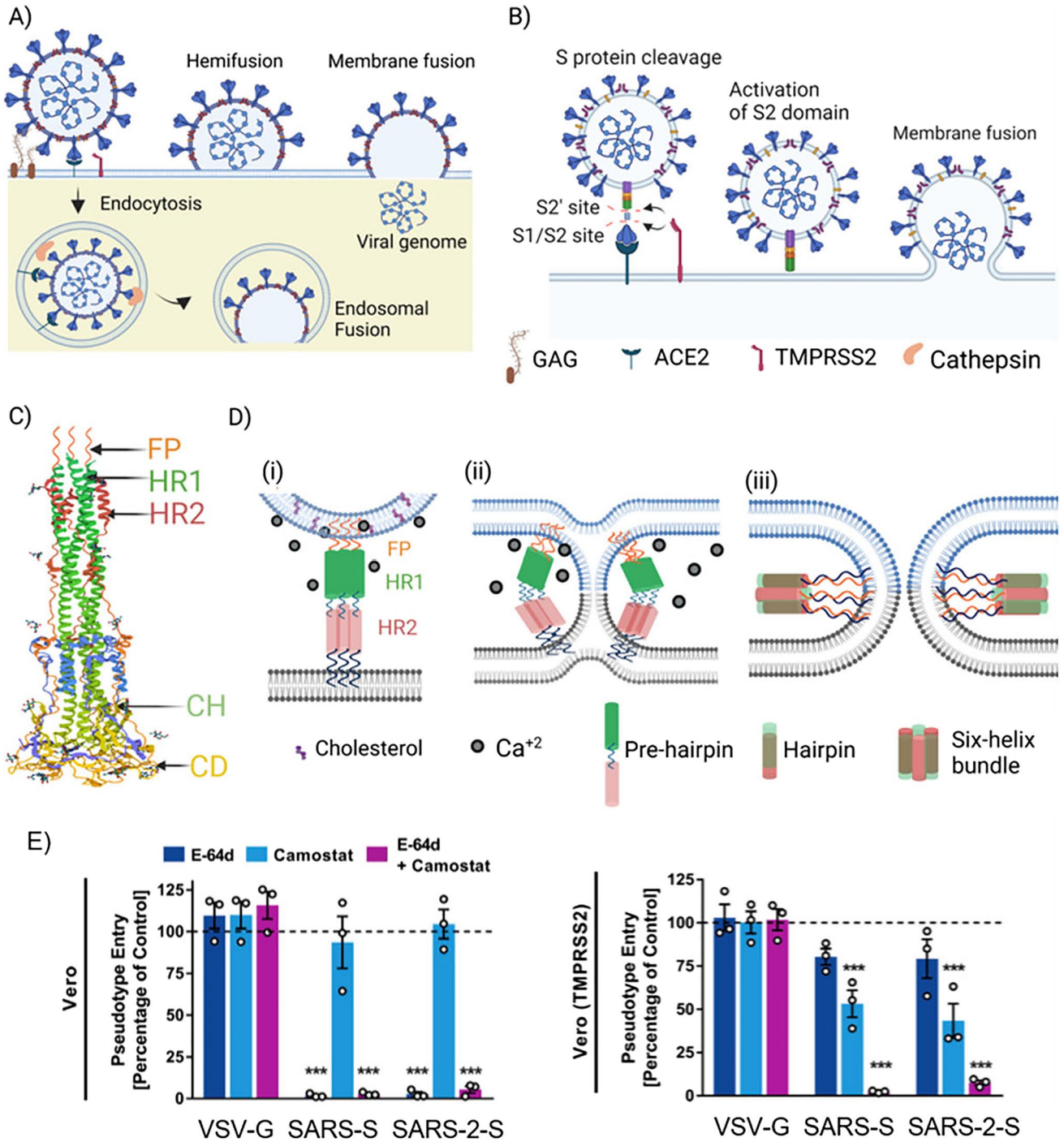


configurational transitions from the pre-hairpin to a hairpin structure of the S2 monomer, and three such S2 hairpins form a stable six-helical bundle (Fig. 10D-iv). During this structural transition, the tethered virus envelope and cell membrane are pulled inwards and merge/fuse (Tang et al. 2020) (Fig. 10D).

**Molecular factors of SARS-CoV-2 fusion** Specific molecular factors and cellular signaling are essential to trigger and carry forward the configurational transitions of the S2. These factors can be pH, divalent ions, cellular proteases, and other cellular or membrane proteins (Lai et al. 2017; Hoffmann et al. 2020b; Pattnaik et al. 2021; Tang et al. 2021). However, the essential molecular and cellular factors for the membrane fusion of SARS-CoV-2 are yet to be confirmed. Also, there is a lack of clarity regarding the fusion pathway that is whether the virus fuses at the plasma membrane or requires a low pH environment of endosomes (Fig. 10A).

◂**Fig. 10** Membrane fusion of SARS-CoV-2. **A** Schematic of the membrane attachment, hemifusion, and fusion of the virions in a host cell. The fusion can occur either at the plasma membrane or in endosomes after cellular entry of the virus via endocytosis. TMPRSS2 and cathepsin are the plasma membrane and endosomal protease, respectively, which involve in the activation of the S protein. **B** Scheme showing the TMPRSS2 assisted proteolytic cleavage of the S protein which is bound to the membrane ACE2. The cleavage causes an activation of the protein which is critical for the conformational changes of the S2 and, thereby, membrane fusion of the virus. S1/S2 site: Arg689/690 and S2′ site: Arg815/Ser816. **C** Structure of the S2 trimer at the post-fusion conformation (Cai et al. 2020). The major domains of the protein which go through conformational transitions during membrane fusion are indicated. FP: fusion peptide; HRs: heptad repeats; CH: central helix; CD: connecting domain. **D** Schemes illustrating (*i*) membrane tethering, (*ii*) hemifusion, and (*iii*) fusion pore opening state. The pre-hairpin to hairpin transition of the S2 protein leads to the membrane fusion state. The hairpin structure appears as a six-helix bundle of the trimeric S2 protein. Cell membrane cholesterol and calcium ion ($Ca.^{2+}$) can have roles in membrane hemifusion and fusion (described in the text). **E** The role of two cellular proteases, i.e., cathepsin and TMPRSS2, for the entry of viruses in host cells (with or without TMPRSS2). E-64d and camostat block the activity of the enzymes, respectively. (**A**)–(**D**) are created with Biorender.com. (**E**) is adapted with permission from Hoffmann et al. (2020b)

Multiple groups have reported that the viral fusion or entry requires priming of the S protein by membrane proteases such as TMPRSS2 and cathepsin (Hoffmann et al. 2020b; Ou et al. 2020) which are expressed in the respiratory cells (Donaldson et al. 2002). The enzyme cleaves two peptide bonds, i.e., Arg689/690 and Arg815/Ser816 at the S1/S2 and S2′ sites, respectively (Gioia et al. 2020; Hoffmann et al. 2020b) (Fig. 10B). Hoffman et al. (2020b) and Ou et al. (2020) investigated the activity of cellular proteases, in particular, a serine protease (TMPRSS2), and cysteine proteases, i.e., cathepsin B and L (Cat B/L), by performing cellular infection studies. TMPRSS2 in the plasma membrane is active at neutral pH, whereas Cat B/L are active only at acidic pH such as in endosomes. The viral entry, as detected via luciferase assay, is partially blocked upon pH-based inactivation of Cat B/L in cells expressing TMPRSS2. Inhibition of either TMPRSS2 or cathepsin enzymes using specific small molecular inhibitors (camostat mesylate, E-64d, etc.) significantly reduces the viral entry in the host cells (Fig. 10E). The viral entry is completely blocked upon inhibition of both enzymes such as upon inactivation of Cat B/L in cells without TMPRSS2. These data indicate that TMPRSS2 of the plasma membrane primes the majority of the S protein and the residual S protein can further be primed by the available cathepsin proteases in endosomes. Depending on the availability of cellular proteases, SARS-CoV-2 can either fuse at the plasma membrane or take endosomal fusion path (Fig. 10A), increasing their chances of cellular entry and transmission.

The enhanced fusogenicity of the virus has also been linked with its furin cleavage site which has multiple arginine (basic) residues (RRAR) at 681–684 position of the S protein (SD domains, near S1/S2 site) (Walls et al. 2020, 2016; Wrapp et al. 2020) (Fig. 8A). It is a unique structural feature of SARS-CoV-2 as other coronaviruses (serbecovirus lineage) contain a monobasic cleavage site (Andersen et al. 2020; Whittaker 2021). The multibasic site is prone to cleavage by ubiquitous furin and furin-like proteases. A similar multibasic furin cleavage site in avian influenza viruses (H5 and H7 subtypes) is known to increase the pathogenicity of the virus. Animal studies using mutated SARS-CoV-2 have shown that the virus has higher infectivity because of the furin cleavage site (Peacock et al. 2021) which facilitates the activation of the S protein and thereby cellular entry of the virions in the endosomal-independent pathway (Fig. 10A, B). This could also be a reason for the virus-mediated cellular syncytia formation in host cells (Hoffmann et al. 2020a; Mykytyn et al. 2021; Peacock et al. 2021). However, multiple cellular studies reported that the multibasic site is not essential for such cell syncytia formation (Ou et al. 2020; Xia et al. 2020a) and cellular infection (Walls et al. 2020) by SARS-CoV-2. Xia et al. (2020a) investigated this by probing the cell–cell fusion induced by virions with or without the multibasic site and observed no major differences in the fusion extent. Walls et al. (2020) showed that the furin-mediated S1/S2 cleavage is not essential for the cellular entry of SARS-CoV-2 (using VeroE6 or BHK cells). Most of the literature has discussed that the multibasic furin cleavage site of the S protein is likely to contribute to expanding the host cell tropism of SARS-CoV-2 (Lan et al. 2020; Walls et al. 2020; Whittaker 2021), but its role in enhanced infectivity and transmissibility of the virus is yet to be confirmed.

ACE2 binding, TMPRSS2 activity, etc. require that these membrane proteins are accessible to virions during their interaction with a host cell. Membrane factors like cholesterol, lipid rafts and membrane rigidity/deformability regulate the distribution of the membrane proteins which in turn determine their accessibility. Recently, Wang et al. employed a super-resolution microscopy (dSTORM) technique to resolve the spatial correlation of ACE2 and lipid rafts (from GM1 distribution) on the plasma membrane of cells infected with pseudotype SARS-CoV-2 (Wang et al. 2021). The authors observed a greater spatial correlation for cells loaded with cholesterol. The infection level in these cells is higher up by ~ 50% and becomes sensitive upon cholesterol depletion.

Similarly, Pattnaik et al. (2021) and Sanders et al. (2021) employed fluorescence spectroscopy tools such as fluorescence resonance energy transfer (FRET) for examining the lipid mixing induced by different fusion peptides (FPs). Their data confirm that increased cholesterol content in artificial lipid vesicles increases the extent of lipid mixing, and this phenomenon is specific to the FP of SARS-CoV-2. High cholesterol content in lipid membranes is associated with $L_o$

domains and lipid rafts which contribute to the greater membrane tension. Such cholesterol-rich lipid vesicles can lower their membrane tension upon fusion (lipid mixing) as triggered by the viral FP. At the cellular level, cholesterol aids in the trafficking of membrane proteins like ACE2 and proteases into lipid rafts (Zang et al. 2020; Sanders et al. 2021). Such protein organization in cell membranes can facilitate the binding and fusion of SARS-CoV-2 at lipid rafts. Thus, an increased cholesterol level may link to a greater chance of the virus attachment to and fusion with host cells (Figs. 9B and 10D-i). This cholesterol dependency of SARS-CoV-2 can be associated with the higher COVID infection among the older population.

Other potential factors for the membrane fusion of SARS-CoV-2 are pH and calcium ion ($Ca^{2+}$) (Tang et al. 2020). While the role of pH is still obscure, recent studies by Lai et al. (2017), Xia et al. (2020b), and others (Straus et al. 2021; Khelashvili et al. 2021) indicate that the FP's activity has a strong dependence on $Ca^{2+}$. The authors corroborated the ion effect by depletion of intracellular and extracellular $Ca^{2+}$ and thereafter, analyzing the cell viability with luminescence assay. The application of a $Ca^{2+}$ chelating agent (EDTA) to infected cells reduces the membrane insertion of the FP and lowers the cellular infection by ~ 2.9-fold. The intracellular $Ca^{2+}$ effect is examined by using a membrane-permeable chelator (BAPTA-AM) which results in a ~ 60-fold decrease in the cellular infection. It is hypothesized that electrostatic interactions between $Ca^{2+}$ and negatively charged headgroup of lipid bilayers overcome the electrostatic barrier during membrane hemifusion and fusion (Fig. 10D-i and ii). Moreover, structural studies reveal that the FP of SARS-CoV-2 binds to two $Ca^{2+}$ at the E819/D820 and D830/D839 sites (Khelashvili et al. 2021). The FP-bound $Ca^{2+}$ can also facilitate the virus fusion by lowering the electrostatic repulsion between the merging membranes.

**Effect of mutation on the structure and function of S protein** Beyond the enhanced attachment and fusion of SARS-CoV-2, rapid mutations of the virus have become a major concern. The mutated strains of the virus such as D614G, Delta, and Omicron are reported to be more transmissive (Harvey et al. 2021; Saxena and Moneim 2022). February 2020 onwards, the COVID-19 pandemic became dominated by the spread of a SARS-CoV-2 variant that is mutated at the 614th position of the S protein, known as D614G (aspartic acid, D to glycine, G). About 1.4- to 5.5-fold more viral load appeared in the URT of COVID patients infected by D614G (Korber et al. 2020). The structure of the mutated S protein indicates the possible reasons behind the enhanced infectivity (Benton et al. 2021; Zhang et al. 2021). For example, Zhang et al. (2021) resolved the structure of the mutated protein using cryo-EM at ~ 3-Å resolution. The variant has an intermediate conformation between the closed and open conformation, i.e., one RBD flipped up only halfway. This causes the variant to attain a relatively more open conformation. Interestingly, the 630th loop (620–640 residues) in its closed conformation appears to be more ordered upon the mutation and experiences hydrophobic interactions with the RBD. However, these changes did not alter the binding strength of the S protein toward ACE2 as the measured $k_D$ is 15.5 and 11.2 nM with and without the mutation, respectively (Zhang et al. 2021). The mutated protein has an additional H-bond between the G614 residue and a lysine residue (K854) at the FP of S2, and it retards the dissociation of the S1 from S2 (Zhang et al. 2021). These structural features indicate that the D614G substitution prevents premature post-fusion of the S protein and increases the percentage of "up" RBD in the trimeric protein, resulting in an efficient membrane attachment and fusion. Recently, Mehra and Kepp (2021) wrote a detailed review on the S-protein mutation and it can be referred to for learning the respective structural details.

## Summary

HIV-1, IAVs, and SARS-CoV-2 pose a recurring threat of pandemics because of their latency, rapid mutation, and transmission. This is why therapeutics to treat infectious diseases caused by these viruses require constant development. The fundamental studies on viral replication including some of the literature which are reviewed in this article have been instrumental in such development. Considerable efforts are being made to design drug molecules which can neutralize the virions (Taylor et al. 2021; Brown et al. 2007) or target the membrane attachment and fusion of the virions (De Clercqa and Li 2016; Tang et al. 2020; Bai et al. 2021; Liu and Yang 2021).

As we reviewed the literature, it is evident that the spike proteins of HIV-1, IAVs, and SARS-CoV-2 are the key to the cellular attachment and membrane fusion of the virions. Irrespective of the different amino acid sequences of the proteins, they share structural features. For example, the bulky head group of the spike protein is dominated by β-sheets and has the RBD, whereas the stalk part is primarily composed of α-helices and contains the FP. More importantly, the structure of the spike protein is highly dynamic as we have discussed the closed and open conformations of the head group, the pre-hairpin and hairpin configurations of the stalk domain, and several other intermediate configurations. These structural dynamics have far-reaching importance in viral replication, in particular, gaining a fine balance between (1) the protection of the conserved RBD and FP from neutralizing antibodies and (2) achieving the receptor binding and triggering the membrane fusion. The applications of X-ray crystallography,

cryo-EM, cryo-ET, smFRET, and other techniques which are not covered in the article such as mass spectrometry and nuclear magnetic resonance have been at the forefront in decoding the structure and configurational dynamics of the spike proteins. The corresponding findings have contributed to the understanding of their structural and functional correlation which is central to the design of antivirals. Small molecules, peptides, and even monoclonal antibodies targeting the RBD, FP or interfering with the RBD–receptor complexation and pre-hairpin to hairpin transition have been successfully applied as antiviral drugs (De Clercq and Li 2016; O'Hanlon and Shaw 2019; Kozal et al. 2020; Liu and Yang 2021; Taylor et al. 2021).

Beyond the structure and function of the spike proteins, it is of fundamental interest to understand how the virions utilize the spike proteins to navigate the crowded cell surface, achieve membrane attachment, and commence membrane fusion. IAVs and SARS-CoV-2 can migrate through the cell surface proteoglycans/mucins to reach the plasma membrane, whereas HIV-1 particles get trapped by them. At the plasma membrane, the receptor binding affinity and multivalent binding play vital roles in achieving membrane attachment of the virions. The spike proteins of HIV-1 and SARS-CoV-2 have a relatively high receptor binding affinity (nanomolar $k_D$), whereas it is much lower for IAVs (millimolar $k_D$). Thereby, a single IAV particle engages in interaction with multiple sialylated receptors. Also, the antagonistic function of HA and NA leads to a complex and dynamic multivalent binding of the virions. Unlike IAVs, the multivalent interaction of HIV-1 and SARS-CoV-2 is less discussed in the literature. The described case studies in this review show that the residence time of HIV-1 increases upon simultaneous interaction with CD4 receptor and CCR5 co-receptor, and a single SARS-CoV-2 particle can form multiple RBD-ACE2 pairs via the "up" RBD of the S protein. Unlike the membrane attachment, the membrane fusion steps of the virions have much in common. The fusion process commences upon the release of FP for membrane tethering followed by configurational transitions of the stalk subunit. Interestingly, successful fusion events of the virions may require multiple releasable FPs. For example, three FPs are essential for the membrane tethering of SARS-CoV-2 and the fusion of IAVs occurs via synergistic or cooperative configurational transitions of HA trimers. Also, the membrane fusion of the virions is substantially affected by cellular factors. In particular, the membrane factors such as the cholesterol content and lipid domains/rafts influence the fusion kinetics of HIV-1 and SARS-CoV-2.

Through our discussed case studies, it is also evident that biophysical techniques like SPR, BLI, AFM, fluorescence imaging, and flow cytometry have been vital in probing the receptor binding affinity, glycan binding, mobility of virions, and kinetics of membrane attachment and fusion. Moreover, it has been possible to resolve or better understand the multivalent binding and synergistic/cooperative transitions upon the application of single-molecule force spectroscopy and single-particle fluorescence imaging techniques. The latter technique in combination with cellular infection studies revealed the cellular factors and the pathways of membrane fusion. Thereby, these specialized biophysical techniques can also be applied to evaluate novel antiviral strategies such as inhibiting the multivalent binding and cooperative configurational transitions or modulating the cellular factors for the membrane attachment and fusion of the virions.

**Acknowledgements** The authors thank Prof. Vladimir Zhadnov for critical reading of the introduction of the article and providing feedback on the main text.

**Author contribution** GN, AS, and MD wrote the sections of SARS-CoV-2, IAVs, and HIV-1, respectively. GD wrote the receptor and glycan binding of HIV-1. NP wrote the introduction and summary and corrected the manuscript. The article was written through contributions of all authors. All authors have given approval to the final version of the manuscript.

**Funding** This work is supported by Science and Engineering Research Board, India (SRG/2020/000969 and SB/S1/Covid-5/2020) and IIT Kanpur for the initiation grant and laboratory support.

## Declarations

**Consent for publication** We have taken the permission for reusing the figures from the published journals. They are referred in each figure caption.

**Conflict of interest** The authors declare no competing interests.

## References

Ahn JH, Kim JM, Hong SP et al (2021) Nasal ciliated cells are primary targets for SARS-CoV-2 replication in the early stage of COVID-19. J Clin Invest 131:1–15. https://doi.org/10.1172/JCI148517

Andersen KG, Rambaut A, Lipkin WI et al (2020) The proximal origin of SARS-CoV-2. Nat Med 26:450–452. https://doi.org/10.1038/s41591-020-0820-9

Bai Y, Jones JC, Wong SS, Zanin M (2021) Antivirals targeting the surface glycoproteins of influenza virus: mechanisms of action and resistance. Viruses 13:1–16. https://doi.org/10.3390/v13040624

Bally M, Block S, Höök F et al (2021) Physicochemical tools for studying virus interactions with targeted cell membranes in a molecular and spatiotemporally resolved context. Anal Bioanal Chem 413:7157–7178. https://doi.org/10.1007/s00216-021-03510-5

Belouzard S, Millet JK, Licitra BN, Whittaker GR (2012) Mechanisms of coronavirus cell entry mediated by the viral spike protein. Viruses 4:1011–1033. https://doi.org/10.3390/v4061011

Benton DJ, Gamblin SJ, Rosenthal PB, Skehel JJ (2020a) Structural transitions in influenza haemagglutinin at membrane fusion pH. Nature 583:150–153. https://doi.org/10.1038/s41586-020-2333-6

Benton DJ, Wrobel AG, Roustan C et al (2021) The effect of the D614G substitution on the structure of the spike glycoprotein of

SARS-CoV-2. Proc Natl Acad Sci U S A 118:2–5. https://doi.org/10.1073/pnas.2022586118
Benton DJ, Wrobel AG, Xu P et al (2020b) Receptor binding and priming of the spike protein of SARS-CoV-2 for membrane fusion. Nature 588:327–330. https://doi.org/10.1038/s41586-020-2772-0
Beumer MC, Koch RM, Van BD et al (2018) Influenza virus and factors that are associated with ICU admission, pulmonary co-infections and ICU mortality. J Crit Care 50:59–65. https://doi.org/10.1016/j.jcrc.2018.11.013
Booy FP, Ruigrok RWH, van Bruggen EFJ (1985) Electron microscopy of influenza virus. A comparison of negatively stained and ice-embedded particles. J Mol Biol 184:667–676. https://doi.org/10.1016/0022-2836(85)90312-2
Böttcher E, Matrosovich T, Beyerle M et al (2006) Proteolytic activation of influenza viruses by serine proteases TMPRSS2 and HAT from human airway epithelium. J Virol 80:9896–9898. https://doi.org/10.1128/jvi.01118-06
Bouvier NM, Palese P (2008) The biology of influenza viruses. Vaccine 26:49–53. https://doi.org/10.1016/j.vaccine.2008.07.039
Brown JR, Crawford BE, Esko JD (2007) Glycan antagonists and inhibitors: a fount for drug discovery. In Critical reviews in Biochem Molec Biol 42(6):481–515
Bullough PA, Hughson FM, Skehel JJ, Wiley DC (1994) Strcuture of influenza haemagglutinin at the pH of membrane fusion. Nature 371:37–43. https://doi.org/10.1038/371037a0
Byrd-Leotis L, Cummings RD, Steinhauer DA (2017) The interplay between the host receptor and influenza virus hemagglutinin and neuraminidase. Int J Mol Sci 18:1–22. https://doi.org/10.3390/ijms18071541
Cai Y, Zhang J, Xiao T et al (2020) Distinct conformational states of SARS-CoV-2 spike protein. Science 369(6511):1586–1592. https://doi.org/10.1126/science.abd4251
Caillat C, Guilligay D, Torralba J et al (2021) Structure of hiv-1 gp41 with its membrane anchors targeted by neutralizing antibodies. Elife 10:1–26. https://doi.org/10.7554/ELIFE.65005
Calder LJ, Rosenthal PB (2016) Cryomicroscopy provides structural snapshots of influenza virus membrane fusion. Nat Struct Mol Biol 23:853–858. https://doi.org/10.1038/nsmb.3271
Campbell EM, Perez O, Melar M, Hope TJ (2007) Labeling HIV-1 virions with two fluorescent proteins allows identification of virions that have productively entered the target cell. Virology 360:286–293. https://doi.org/10.1016/j.virol.2006.10.025
Casalino L, Gaieb Z, Goldsmith JA et al (2020) Beyond shielding: the roles of glycans in the SARS-CoV-2 spike protein. ACS Cent Sci 6:1722–1734. https://doi.org/10.1021/acscentsci.0c01056
Chan DC, Fass D, Berger JM, Kim PS (1997) Core structure of gp41 from the HIV envelope glycoprotein. Cell 89:263–273. https://doi.org/10.1016/S0092-8674(00)80205-6
Chang MI, Panorchan P, Dobrowsky TM et al (2005) Single-molecule analysis of human immunodeficiency virus type 1 gp120-receptor interactions in living cells. J Virol 79:14748–14755. https://doi.org/10.1128/jvi.79.23.14748-14755.2005
Chen YC, Sood C, Marin M et al (2020) Super-resolution fluorescence imaging reveals that serine incorporator protein 5 inhibits human immunodeficiency virus fusion by disrupting envelope glycoprotein clusters. ACS Nano 14:10929–10943. https://doi.org/10.1021/acsnano.0c02699
Chinen J, Shearer WT (2002) Molecular virology and immunology of HIV infection. J Allergy Clin Immunol 110:189–198. https://doi.org/10.1067/mai.2002.126226
Chu H, Chan JF-W, Yuen TT-T et al (2020) Comparative tropism, replication kinetics, and cell damage profiling of SARS-CoV-2 and SARS-CoV with implications for clinical manifestations, transmissibility, and laboratory studies of COVID-19: an observational study. The Lancet Microbe 1:e14–e23. https://doi.org/10.1016/s2666-5247(20)30004-5
Chu VC, Whittaker GR (2004) Influenza virus entry and infection require host cell N-linked glycoprotein. Proc Natl Acad Sci 101:18153–18158. https://doi.org/10.1073/pnas.0405172102
Clausen TM, Sandoval DR, Spliid CB et al (2020) SARS-CoV-2 infection depends on cellular heparan sulfate and ACE2. Cell 183:1043-1057.e15. https://doi.org/10.1016/j.cell.2020.09.033
Connell BJ, Lortat-Jacob H (2013) Human immunodeficiency virus and heparan sulfate: from attachment to entry inhibition. Front Immunol 4:1–12. https://doi.org/10.3389/fimmu.2013.00385
Coomer CA, Carlon-Andres I, Iliopoulou M et al (2020) Single-cell glycolytic activity regulates membrane tension and HIV-1 fusion. PLoS Pathog 16:1–31. https://doi.org/10.1371/journal.ppat.1008359
Costello DA, Lee DW, Drewes J et al (2012) Influenza virus-membrane fusion triggered by proton uncaging for single particle studies of fusion kinetics. Anal Chem 84:8480–8489. https://doi.org/10.1021/ac3006473
Costello DA, Whittaker GR, Daniel S (2015) Variations in pH sensitivity, acid stability, and fusogenicity of three influenza virus H3 subtypes. J Virol 89:350–360. https://doi.org/10.1128/jvi.01927-14
Daecke J, Fackler OT, Dittmar MT (2005) Involvement of clathrin-mediated endocytosis in human immunodeficiency virus type 1 entry. J Virol 79:1581–1594. https://doi.org/10.1128/JVI.79.3.1581
Das A, Vishvakarma V, Dey A et al (2021) Biophysical properties of the isolated spike protein binding helix of human ACE2. Biophys J 120:2785–2792. https://doi.org/10.1016/j.bpj.2021.06.017
Das DK, Govindan R, Nikić-Spiegel I et al (2018) Direct visualization of the conformational dynamics of single influenza hemagglutinin trimers. Cell 174:926-937.e12. https://doi.org/10.1016/j.cell.2018.05.050
De CE, Li G (2016) Approved antiviral drugs over the past 50 years. Clin Microbiol Rev 29:695–747. https://doi.org/10.1128/CMR.00102-15
De Clercq E, Li G (2016) Approved antiviral drugs over the past 50 years. Clin Microbiol Rev 29:695–747. https://doi.org/10.1128/CMR.00102-15
de la Vega M, Marin M, Kondo N et al (2011) Inhibition of HIV-1 endocytosis allows lipid mixing at the plasma membrane, but not complete fusion. Retrovirology 8:99. https://doi.org/10.1186/1742-4690-8-99
De Vries E, De Vries RP, Wienholts MJ et al (2012) Influenza A virus entry into cells lacking sialylated N-glycans. Proc Natl Acad Sci U S A 109:7457–7462. https://doi.org/10.1073/pnas.1200987109
de Vries E, Du W, Guo H, de Haan CAM (2020) Influenza A virus hemagglutinin–neuraminidase–receptor balance: preserving virus motility. Trends Microbiol 28:57–67. https://doi.org/10.1016/j.tim.2019.08.010
Delaveris CS, Webster ER, Banik SM et al (2020) Membrane-tethered mucin-like polypeptides sterically inhibit binding and slow fusion kinetics of influenza A virus. Proc Natl Acad Sci U S A 117:12643–12650. https://doi.org/10.1073/pnas.1921962117
Delguste M, Zeippen C, Machiels B et al (2018) Multivalent binding of herpesvirus to living cells is tightly regulated during infection. Sci Adv 4:1–12. https://doi.org/10.1126/sciadv.aat1273
Desai TM, Marin M, Chin CR, Savidis G, Brass AL, Melikyan GB (2014) IFITM3 restricts Influenza A virus entry by blocking the formation of fusion pores following virus-endosome hemifusion. PLOS Pathog 10(4):e1004048. https://doi.org/10.1371/journal.ppat.1004048
Dodero-Rojas E, Onuchic JN, Whitford PC (2021) Sterically confined rearrangements of SARS-CoV-2 spike protein control cell invasion. Elife 10:1–26. https://doi.org/10.7554/eLife.70362
Donaldson SH, Hirsh A, Li DC et al (2002) Regulation of the epithelial sodium channel by serine proteases in human airways. J Biol Chem 277:8338–8345. https://doi.org/10.1074/jbc.M105044200

Dou D, Revol R, Östbye H et al (2018) Influenza A virus cell entry, replication, virion assembly and movement. Front Immunol 9:1–17. https://doi.org/10.3389/fimmu.2018.01581

Dutta S, Panthi B, Chandra A (2022) All-atom simulations of human ACE2-spike protein RBD complexes for SARS-CoV-2 and some of its variants: nature of interactions and free energy diagrams for dissociation of the protein complexes. J Phys Chem B 126:5375–5389. https://doi.org/10.1021/acs.jpcb.2c00833

Eisen MB, Sabesan S, Skehel JJ, Wiley DC (1997) Binding of the influenza A virus to cell-surface receptors: structures of five hemagglutinin-sialyloligosaccharide complexes determined by X-ray crystallography. Virology 232:19–31. https://doi.org/10.1006/viro.1997.8526

Endreß T, Lampe M, Briggs JAG et al (2008) HIV-1-cellular interactions analyzed by single virus tracing. Eur Biophys J 37:1291–1301. https://doi.org/10.1007/s00249-008-0322-z

Fei Y, Sun YS, Li Y et al (2015) Characterization of receptor binding profiles of influenza a viruses using an ellipsometry-based label-free glycan microarray assay platform. Biomolecules 5:1480–1498. https://doi.org/10.3390/biom5031480

Fera A, Farrington JE, Zimmerberg J, Reese TS (2012) A negative stain for electron microscopic tomography. Microsc Microanal 18:331–335. https://doi.org/10.1017/S1431927611012797

Firrito C, Bertelli C, Vanzo T et al (2018) SERINC5 as a new restriction factor for human immunodeficiency virus and murine leukemia virus. Annu Rev Virol 5(1):323–340. https://doi.org/10.1146/annurev-virology-092917-043308

Floyd DL, Ragains JR, Skehel JJ et al (2008) Single-particle kinetics of influenza virus membrane fusion. Proc Natl Acad Sci U S A 105:15382–15387. https://doi.org/10.1073/pnas.0807771105

Fontana J, Cardone G, Heymann J, Bernard W, Dennis C, Steven AC (2012) Structural changes in influenza virus at low pH characterized by cryo-electron tomography. J Virol 86:2919–2929. https://doi.org/10.1017/S1431927612002395

Fredericksen BL, Wei BL, Yao J et al (2002) Inhibition of endosomal/lysosomal degradation increases the infectivity of human immunodeficiency virus. J Virol 76:11440–11446. https://doi.org/10.1128/jvi.76.22.11440-11446.2002

Friedrich BM, Dziuba N, Li G et al (2011) Host factors mediating HIV-1 replication. Virus Res 161:101–114. https://doi.org/10.1016/j.virusres.2011.08.001

Gioia M, Ciaccio C, Calligari P et al (2020) Role of proteolytic enzymes in the COVID-19 infection and promising therapeutic approaches. Biochem Pharmacol 182:114225–114246. https://doi.org/10.1016/j.bcp.2020.114225

Gui L, Ebner JL, Mileant A et al (2016) Visualization and sequencing of membrane remodeling leading to influenza virus fusion. J Virol 90:6948–6962. https://doi.org/10.1128/jvi.00240-16

Gunnarsson A, Dexlin L, Wallin P et al (2011) Kinetics of ligand binding to membrane receptors from equilibrium fluctuation analysis of single binding events. J Am Chem Soc 133:14852–14855. https://doi.org/10.1021/ja2047039

Haldar S, Okamoto K, Dunning RA, Kasson PM (2020) Precise triggering and chemical control of single-virus fusion within endosomes. J Virol 95:1–10. https://doi.org/10.1128/jvi.01982-20

Hallenberger S, Bosch V, Angliker H, Klenk HD, Garten W (1992) Inhibition of furin-mediated cleavage activation of HIV-1 glycoprotein gp 160. Nature 360(6402):358–361. https://doi.org/10.1038/255243a0

Hamilton BS, Whittaker GR, Daniel S (2012) Influenza virus-mediated membrane fusion: determinants of hemagglutinin fusogenic activity and experimental approaches for assessing virus fusion. Viruses 4:1144–1168. https://doi.org/10.3390/v4071144

Hamming I, Timens W, Bulthuis MLC et al (2004) Tissue distribution of ACE2 protein, the functional receptor for SARS coronavirus. A first step in understanding SARS pathogenesis. J Pathol 203:631–637. https://doi.org/10.1002/path.1570

Hanley W, McCarty O, Jadhav S et al (2003) Single molecule characterization of P-selectin/ligand binding. J Biol Chem 278:10556–10561. https://doi.org/10.1074/jbc.M213233200

Harris A, Borgnia MJ, Shi D et al (2011) Trimeric HIV-1 glycoprotein gp140 immunogens and native HIV-1 envelope glycoproteins display the same closed and open quaternary molecular architectures. Proc Natl Acad Sci U S A 108:11440–11445. https://doi.org/10.1073/pnas.1101414108

Harris A, Cardone G, Winkler DC et al (2006) Influenza virus pleiomorphy characterized by cryoelectron tomography. Proc Natl Acad Sci U S A 103:19123–19127. https://doi.org/10.1073/pnas.0607614103

Harris AK, Meyerson JR, Matsuoka Y et al (2013) Structure and accessibility of HA trimers on intact 2009 H1N1 pandemic influenza virus to stem region-specific neutralizing antibodies. Proc Natl Acad Sci U S A 110:4592–4597. https://doi.org/10.1073/pnas.1214913110

Harrison AG, Lin T, Wang P (2020) Mechanisms of SARS-CoV-2 transmission and pathogenesis. Trends Immunol 41:1100–1115. https://doi.org/10.1016/j.it.2020.10.004

Harrison SC (2005) Mechanism of membrane fusion by viral envelope proteins. Adv Virus Res 64:231–261

Harrison SC (2008) Viral membrane fusion. Nat Struct Mol Biol 15:690–698. https://doi.org/10.1038/nsmb.1456

Harvey WT, Carabelli AM, Jackson B et al (2021) SARS-CoV-2 variants, spike mutations and immune escape. Nat Rev Microbiol 19:409–424. https://doi.org/10.1038/s41579-021-00573-0

Helenius A (2018) Virus entry: looking back and moving forward. J Mol Biol 430:1853–1862. https://doi.org/10.1016/j.jmb.2018.03.034Edited

Henderson R, Edwards RJ, Mansouri K et al (2020) Controlling the SARS-CoV-2 spike glycoprotein conformation. Nat Struct Mol Biol 27:925–933. https://doi.org/10.1038/s41594-020-0479-4

Herschhorn A, Finzi A, Jones DM et al (2011) An inducible cell-cell fusion system with integrated ability to measure the efficiency and specificity of HIV-1 entry inhibitors. PLoS ONE 6:26731–26745. https://doi.org/10.1371/journal.pone.0026731

Hoffmann M, Kleine-Weber H, Pöhlmann S (2020a) A multibasic cleavage site in the spike protein of SARS-CoV-2 is essential for infection of human lung cells. Mol Cell 78:779-784.e5. https://doi.org/10.1016/j.molcel.2020.04.022

Hoffmann M, Kleine-Weber H, Schroeder S et al (2020b) SARS-CoV-2 cell entry depends on ACE2 and TMPRSS2 and is blocked by a clinically proven protease inhibitor. Cell 181:271–280. https://doi.org/10.1016/j.cell.2020.02.052

Honigfort DJ, Altman MO, Gagneux P, Godula K (2021) Glycocalyx crowding with mucin mimetics strengthens binding of soluble and virus-associated lectins to host cell glycan receptors. Proc Natl Acad Sci U S A 118:1–8. https://doi.org/10.1073/pnas.2107896118

Hou YJ, Okuda K, Edwards CE et al (2020) SARS-CoV-2 reverse genetics reveals a variable infection gradient in the respiratory tract. Cell 182:429–446. https://doi.org/10.1016/j.cell.2020.05.042

Howard AR, Monru JB (2019) Developments in single-molecule and single-particle fluorescence-based approaches for studying viral envelope glycoprotein dynamics and membrane fusion. Adv Virus Res 104:123–146. https://doi.org/10.1016/bs.aivir.2019.05.004

Huang CC, Tang M, Zhang MY et al (2005) Structural biology: structure of a V3-containing HIV-1 gp120 core. Science 310(5750):1025–1028. https://doi.org/10.1126/science.1118398

Huang Y, Yang C, feng X et al (2020) Structural and functional properties of SARS-CoV-2 spike protein: potential antivirus drug

development for COVID-19. Acta Pharmacol Sin 41:1141–1149. https://doi.org/10.1038/s41401-020-0485-4
Ivanovic T, Choi JL, Whelan SP et al (2013) Influenza-virus membrane fusion by cooperative fold-back of stochastically induced hemagglutinin intermediates. Elife 2013:1–20. https://doi.org/10.7554/eLife.00333
Ivanovic T, Harrison SC (2015) Distinct functional determinants of influenza hemagglutinin-mediated membrane fusion. Elife 4:1–24. https://doi.org/10.7554/eLife.11009
Jackson CB, Farzan M, Chen B, Choe H (2022) Mechanisms of SARS-CoV-2 entry into cells. Nat Rev Mol Cell Biol 23:3–20. https://doi.org/10.1038/s41580-021-00418-x
Janes PW, Ley SC, Magee AI (1999) Aggregation of lipid rafts accompanies signaling via the T cell antigen receptor. J Cell Biol 147:447–461. https://doi.org/10.1083/jcb.147.2.447
Kalathiya U, Padariya M, Mayordomo M, Lisowska M, Nicholson J, Singh A, Baginski M, Fahraeus R, Carragher N, Ball K, Haas J, Daniels A, Hupp TR, Alfaro JA (2020) Highly conserved homotrimer cavity formed by the SARS-CoV-2 spike glycoprotein: a novel binding site. J Clin Med 9(5):1473. https://doi.org/10.3390/jcm9051473
Ke Z, Oton J, Qu K et al (2020) Structures and distributions of SARS-CoV-2 spike proteins on intact virions. Nature 588:498–502. https://doi.org/10.1038/s41586-020-2665-2
Khelashvili G, Plante A, Doktorova M, Weinstein H (2021) Ca2+-dependent mechanism of membrane insertion and destabilization by the SARS-CoV-2 fusion peptide. Biophys J 120:1105–1119. https://doi.org/10.1016/j.bpj.2021.02.023
Kielian M (2020) Enhancing host cell infection by SARS-CoV-2. Science 370(6518):765–766. https://doi.org/10.1126/science.abf0732
Kim SP, Chan DC (1998) HIV entry and its inhibition minireview. Cell 93:681–684. https://doi.org/10.1021/ja01618a044
Kim SY, Jin W, Sood A et al (2020) Characterization of heparin and severe acute respiratory syndrome-related coronavirus 2 (SARS-CoV-2) spike glycoprotein binding interactions. Antiviral Res 181:104873–104882. https://doi.org/10.1016/j.antiviral.2020.104873
Klein S, Cortese M, Winter SL et al (2020) SARS-CoV-2 structure and replication characterized by in situ cryo-electron tomography. Nat Commun 11:1–10. https://doi.org/10.1038/s41467-020-19619-7
Klenk HD, Rott R, Orlich M, Blödorn J (1975) Activation of influenza A viruses by trypsin treatment. Virology 68:426–439. https://doi.org/10.1016/0042-6822(75)90284-6
Koehler M, Delguste M, Sieben C et al (2020) Initial step of virus entry: virion binding to cell-surface glycans. Annu Rev Virol 7:143–165. https://doi.org/10.1146/annurev-virology-122019-070025
Korber B, Fischer WM, Gnanakaran S et al (2020) Tracking changes in SARS-CoV-2 spike: evidence that D614G increases infectivity of the COVID-19 virus. Cell 182:812-827.e19. https://doi.org/10.1016/j.cell.2020.06.043
Kosik I, Yewdell JW (2019) Influenza hemagglutinin and neuraminidase: yin–yang proteins coevolving to thwart immunity. Viruses 11:1–18. https://doi.org/10.3390/v11040346
Kozal M, Aberg J, Pialoux G et al (2020) Fostemsavir in adults with multidrug-resistant HIV-1 infection. N Engl J Med 382:1232–1243. https://doi.org/10.1056/nejmoa1902493
Kwon YD, Finzi A, Wu X, Dogo-Isonagie C, Lee LK, Moore LR, Schmidt SD, Stuckey J, Yang Y, Zhou T, Zhu J, Vicic DA, Debnath AK, Shapiro L, Bewley CA, Mascola JR, Sodroski JG, Kwong PD (2012) Unliganded HIV-1 gp120 core structures assume the CD4-bound conformation with regulation by quaternary interactions and variable loops. Proc Natl Acad Sci U S A 109:5663–5668. https://doi.org/10.1073/pnas.1112391109
Kwon YD, Pancera M, Acharya P, Georgiev IS, Crooks ET, Gorman J, Joyce MG, Guttman M, Ma X, Narpala S, Soto C, Terry DS, Yang Y, Zhou T, Ahlsen G, Bailer RT, Chambers M, Chuang GY, Doria-Rose NA, Druz A, Hallen MA, Harned A, Kirys T, Louder MK, O'Dell S, Ofek G, Osawa K, Prabhakaran M, Sastry M, Stewart-Jones GBE, Stuckey J, Thomas PV, Tittley T, Williams C, Zhang B, Zhao H, Zhou Z, Donald BR, Lee LK, Zolla-Pazner S, Baxa U, Schön A, Freire E, Shapiro L, Lee KK, Arthos J, Munro JB, Blanchard SC, Mothes W, Binley JM, McDermott AB, Mascola JR, Kwong PD (2015) Crystal structure, conformational fixation and entry-related interactions of mature ligand-free HIV-1 Env. Nat Struct Mol Biol 22:522–535. https://doi.org/10.1038/nsmb.3051
Kwong PD, Wyatt R, Robinson J et al (1998) Structure of an HIV gp120 envelope glycoprotein in complex with the CD4 receptor and a neutralizing human antibody. Nature 393:648–659. https://doi.org/10.1038/31405.Structure
Kyriakidis NC, López-Cortés A, González EV et al (2021) SARS-CoV-2 vaccines strategies a comprehensive review of phase 3 candidates. Npj Vaccines 6:1–17. https://doi.org/10.1038/s41541-021-00292-w
Lai AL, Millet JK, Daniel S et al (2017) The SARS-CoV fusion peptide forms an extended bipartite fusion platform that perturbs membrane order in a calcium-dependent manner. J Mol Biol 429:3875–3892. https://doi.org/10.1016/j.jmb.2017.10.017
Lampe M, Briggs JAG, Endress T et al (2007) Double-labelled HIV-1 particles for study of virus-cell interaction. Virology 360:92–104. https://doi.org/10.1016/j.virol.2006.10.005
Lan J, Ge J, Yu J et al (2020) Structure of the SARS-CoV-2 spike receptor-binding domain bound to the ACE2 receptor. Nature 581:215–220. https://doi.org/10.1038/s41586-020-2180-5
Lee KK (2010) Architecture of a nascent viral fusion pore. EMBO J 29:1299–1311. https://doi.org/10.1038/emboj.2010.13
Li F (2016) Structure, function, and evolution of coronavirus spike proteins. Annu Rev Virol 3:237–261. https://doi.org/10.1146/annurev-virology-110615-042301
Li K, Markosyan RM, Zheng YM et al (2013) IFITM proteins restrict viral membrane hemifusion. PLoS Pathog 9:1003124–1003142. https://doi.org/10.1371/journal.ppat.1003124
Li Z, Li W, Lu M et al (2020) Subnanometer structures of HIV-1 envelope trimers on aldrithiol-2-inactivated virus particles. Nat Struct Mol Biol 27:726–734. https://doi.org/10.1038/s41594-020-0452-2
Liu HY, Yang PL (2021) Small-molecule inhibition of viral fusion glycoproteins. Annu Rev Virol 8:459–489. https://doi.org/10.1146/annurev-virology-022221-063725
Liu J, Bartesaghi A, Borgnia MJ et al (2008) Molecular architecture of native HIV-1 gp120 trimers. Nature 455:109–113. https://doi.org/10.1038/nature07159
Liu KN, Boxer SG (2020) Target membrane cholesterol modulates single influenza virus membrane fusion efficiency but not rate. Biophys J 118:2426–2433. https://doi.org/10.1016/j.bpj.2020.03.021
Liu L, Chopra P, Li X et al (2021) Heparan sulfate proteoglycans as attachment factor for SARS-CoV-2. ACS Cent Sci 7:1009–1018. https://doi.org/10.1021/acscentsci.1c00010
Liu SL, Wang ZG, Xie HY et al (2020) Single-virus tracking: from imaging methodologies to virological applications. Chem Rev 120:1936–1979. https://doi.org/10.1021/acs.chemrev.9b00692
Llorente García I, Marsh M (2020) A biophysical perspective on receptor-mediated virus entry with a focus on HIV. Biochim Biophys Acta - Biomembr 1862:1–21. https://doi.org/10.1016/j.bbamem.2019.183158
Lu M, Ma X, Castillo-menendez LR et al (2019) Associating HIV-1 envelope glycoprotein structures with states on the virus observed by smFRET. Nature 568:415–419. https://doi.org/10.1038/s41586-019-1101-y.Associating

Lu M, Uchil PD, Li W et al (2020) Real-time conformational dynamics of SARS-CoV-2 spikes on virus particles. Cell Host Microbe 28:880-891.e8. https://doi.org/10.1016/j.chom.2020.11.001

Lu X, Zhang F, McNew JA, Shin YK (2005) Membrane fusion induced by neuronal SNAREs transits through hemifusion. J Biol Chem 280:30538–30541. https://doi.org/10.1074/jbc.M506862200

Lui I, Zhou XX, Lim SA, Elledge SK, Solomon P, Rettko NJ, Zha BS, Kirkemo LL, Gramespacher JA, Liu J, Muecksch F, Lorenzi JCC, Schmidt F, Weisblum Y, Robbiani DF, Nussenzweig MC, Hatziioannou T, Bieniasz PD, Rosenburg OS, Leung KK, Wells JA (2020) Trimeric SARS-CoV-2 Spike interacts with dimeric ACE2 with limited intra-Spike avidity. https://doi.org/10.1101/2020.05.21.109157

Ma X, Lu M, Gorman J et al (2018) HIV-1 Env trimer opens through an asymmetric intermediate in which individual protomers adopt distinct conformations. Elife 7:1–18. https://doi.org/10.7554/eLife.34271

Mangala Prasad V, Leaman DP, Lovendahl KN et al (2022) Cryo-ET of Env on intact HIV virions reveals structural variation and positioning on the Gag lattice. Cell 185:641–653. https://doi.org/10.1016/j.cell.2022.01.013

Mao Y, Wang L, Gu C et al (2013) Molecular architecture of the uncleaved HIV-1 envelope glycoprotein trimer. Proc Natl Acad Sci U S A 110:12438–12443. https://doi.org/10.1073/pnas.1307382110

Maréchal V, Prevost M-C, Petit C et al (2001) Human immunodeficiency virus type 1 entry into macrophages mediated by macropinocytosis. J Virol 75:11166–11177. https://doi.org/10.1128/jvi.75.22.11166-11177.2001

Mason RJ (2020) Pathogenesis of COVID-19 from a cell biology perspective. Eur Respir J 55:9–11. https://doi.org/10.1183/13993003.00607-2020

Masso M, Vaisman II (2010) Accurate and efficient gp120 V3 loop structure based models for the determination of HIV-1 co-receptor usage. BMC Bioinformatics 11:494. https://doi.org/10.1186/1471-2105-11-494

Matrosovich M, Herrler G, Klenk HD (2013) Sialic acid receptors of viruses. Top Curr Chem 310:1–26. https://doi.org/10.1007/128

Matrosovich MN, Gambaryan AS (2012) Solid-phase assays of receptor-binding specificity. Methods Mol Biol 865:71–95. https://doi.org/10.1007/978-1-61779-621-0

Matsuoka Y, Swayne DE, Thomas C et al (2009) Neuraminidase stalk length and additional glycosylation of the hemagglutinin influence the virulence of influenza H5N1 viruses for mice. J Virol 83:4704–4708. https://doi.org/10.1128/jvi.01987-08

Mayr J, Lau K, Lai JCC et al (2018) Unravelling the role of O-glycans in influenza A virus infection. Sci Rep 8:1–12. https://doi.org/10.1038/s41598-018-34175-3

McAuley JL, Corcilius L, Tan HX et al (2017) The cell surface mucin MUC1 limits the severity of influenza A virus infection. Mucosal Immunol 10:1581–1593. https://doi.org/10.1038/mi.2017.16

Mehra R, Kepp KP (2021) Structure and mutations of SARS-CoV-2 spike protein: a focused overview. ACS Infect Dis 8:29–58. https://doi.org/10.1021/acsinfecdis.1c00433

Melikyan GB (2011) Membrane fusion mediated by human immunodeficiency virus envelope glycoprotein. Curr Top Membr 68:81–106. https://doi.org/10.1016/B978-0-12-385891-7.00004-0

Melikyan GB (2008) Common principles and intermediates of viral protein-mediated fusion: the HIV-1 paradigm. Retrovirology 5:1–13. https://doi.org/10.1186/1742-4690-5-111

Mercer J, Schelhaas M, Helenius A (2010) Virus entry by endocytosis. Annu Rev Biochem 79:803–833. https://doi.org/10.1146/annurev-biochem-060208-104626

Merk A, Subramaniam S (2013) HIV-1 envelope glycoprotein structure. Curr Opin Struct Biol 23:268–276. https://doi.org/10.1016/j.sbi.2013.03.007

Miyauchi K, Kim Y, Latinovic O et al (2009) HIV enters cells via endocytosis and dynamin-dependent fusion with endosomes. Cell 137:433–444. https://doi.org/10.1016/j.cell.2009.02.046

Mori T, Jung J, Kobayashi C et al (2021) Elucidation of interactions regulating conformational stability and dynamics of SARS-CoV-2 S-protein. Biophys J 120:1060–1071. https://doi.org/10.1016/j.bpj.2021.01.012

Mulay A, Konda B, Garcia G et al (2021) SARS-CoV-2 infection of primary human lung epithelium for COVID-19 modeling and drug discovery. Cell Rep 35:1–16. https://doi.org/10.1016/j.celrep.2021.109055

Müller M, Lauster D, Wildenauer HHK et al (2019) Mobility-based quantification of multivalent virus-receptor interactions: new insights into influenza A virus binding mode. Nano Lett 19:1875–1882. https://doi.org/10.1021/acs.nanolett.8b04969

Munro JB, Gorman J, Ma X et al (2014) Conformational dynamics of single HIV-1 envelope trimers on the surface of native virions. Science 346(6210):759–763. https://doi.org/10.1126/science.1254426

Murali S, Rustandi RR, Zheng X et al (2022) Applications of surface plasmon resonance and biolayer interferometry for virus–ligand binding. Viruses 14:1–22. https://doi.org/10.3390/v14040717

Murata K, Wolf M (2018) Cryo-electron microscopy for structural analysis of dynamic biological macromolecules. Biochim Biophys Acta - Gen Subj 1862:324–334. https://doi.org/10.1016/j.bbagen.2017.07.020

Mycroft-West CJ, Su D, Pagani I et al (2020) Heparin inhibits cellular invasion by SARS-CoV-2: structural dependence of the interaction of the Spike S1 receptor-binding domain with heparin. Thromb Haemost 120:1700–1715. https://doi.org/10.1055/s-0040-1721319

Mykytyn AZ, Breugem TI, Riesebosch S et al (2021) SARS-CoV-2 entry into human airway organoids is serine protease-mediated and facilitated by the multibasic cleavage site. Elife 10:1–23. https://doi.org/10.7554/ELIFE.64508

Myszka DG, Sweet RW, Hensley P et al (2000) Energetics of the HIV gp120-CD4 binding reaction. Proc Natl Acad Sci U S A 97:9026–9031. https://doi.org/10.1073/pnas.97.16.9026

Ni F, Chen X, Shen J, Wang Q (2014) Structural insights into the membrane fusion mechanism mediated by influenza virus hemagglutinin. Biochemistry 53:846–854. https://doi.org/10.1021/bi401525h

O'Hanlon R, Shaw ML (2019) Baloxavir marboxil: the new influenza drug on the market. Curr Opin Virol 35:14–18. https://doi.org/10.1016/j.coviro.2019.01.006

Ou X, Liu Y, Lei X et al (2020) Characterization of spike glycoprotein of SARS-CoV-2 on virus entry and its immune cross-reactivity with SARS-CoV. Nat Commun 11:1–12. https://doi.org/10.1038/s41467-020-15562-9

Padilla-Parra S, Marin M, Gahlaut N et al (2013) Fusion of mature HIV-1 particles leads to complete release of a Gag-GFP-based content marker and raises the intraviral pH. PLoS ONE 8:1–16. https://doi.org/10.1371/journal.pone.0071002

Pak AJ, Yu A, Ke Z et al (2022) Cooperative multivalent receptor binding promotes exposure of the SARS-CoV-2 fusion machinery core. Nat Commun 13:1–12. https://doi.org/10.1038/s41467-022-28654-5

Pancera M, Majeed S, Ban YEA et al (2010) Structure of HIV-1 gp120 with gp41-interactive region reveals layered envelope architecture and basis of conformational mobility. Proc Natl Acad Sci U S A 107:1166–1171. https://doi.org/10.1073/pnas.0911004107

Parveen N, Borrenberghs D, Rocha S, Hendrix J (2018) Single viruses on the fluorescence microscope: imaging molecular mobility, interactions and structure sheds new light on viral replication. Viruses 10:1–21. https://doi.org/10.3390/v10050250

Parveen N, Rydell GE, Larson G et al (2019) Competition for membrane receptors: norovirus detachment via lectin attachment. J Am Chem Soc 141:16303–16311. https://doi.org/10.1021/jacs.9b06036

Pattnaik GP, Bhattacharjya S, Chakraborty H (2021) Enhanced cholesterol-dependent hemifusion by internal fusion peptide 1 of SARS coronavirus-2 compared to its N-terminal counterpart. Biochemistry 60:559–562. https://doi.org/10.1021/acs.biochem.1c00046

Pauza CD, Price TM (1988) Human immunodeficiency virus infection of T cells and manocytes proceeds via receptor-mediated endocytosis. J Cell Biol 107:959–968. https://doi.org/10.1083/jcb.107.3.959

Peacock TP, Goldhill DH, Zhou J et al (2021) The furin cleavage site in the SARS-CoV-2 spike protein is required for transmission in ferrets. Nat Microbiol 6:899–909. https://doi.org/10.1038/s41564-021-00908-w

Prabakaran P, Dimitrov AS, Fouts TR, Dimitrov DS (2007) Structure and function of the HIV envelope glycoprotein as entry mediator, vaccine immunogen, and target for inhibitors. Adv Pharmacol 55:33–97. https://doi.org/10.1016/S1054-3589(07)55002-7

Rashid A, Li K, Feng Y et al (2022) HIV-1 genetic diversity a challenge for AIDS vaccine development: a retrospective bibliometric analysis. Hum Vaccines Immunother 18:2014733–2014744. https://doi.org/10.1080/21645515.2021.2014733

Rogers GN, Paulson JC (1983) Receptor determinants of human and animal influenza virus isolates: differences in receptor specificity of the H3 hemagglutinin based on species of origin. Virology 127:361–373. https://doi.org/10.1016/0042-6822(83)90150-2

Roy S, Jaiswar A, Sarkar R (2020) Dynamic asymmetry exposes 2019-nCoV prefusion spike. J Phys Chem Lett 11:7021–7027. https://doi.org/10.1021/acs.jpclett.0c01431

Sakai T, Nishimura SI, Naito T, Saito M (2017) Influenza A virus hemagglutinin and neuraminidase act as novel motile machinery. Sci Rep 7:1–11. https://doi.org/10.1038/srep45043

Sanders DW, Jumper CC, Ackerman PJ et al (2021) Sars-CoV-2 requires cholesterol for viral entry and pathological syncytia formation. Elife 10:1–47. https://doi.org/10.7554/ELIFE.65962

Sauter NK, Hanson JE, Glick GD et al (1992) Binding of influenza virus hemagglutinin to analogs of its cell-surface receptor, sialic acid: analysis by proton nuclear magnetic resonance spectroscopy and X-ray crystallography. Biochemistry 31:9609–9621. https://doi.org/10.1021/bi00155a013

Saxena SK, Moneim ASA (2022) Characterization of the novel SARS-CoV-2 Omicron ( B. 1. 1. 529) variant of concern and its global perspective. J Med Virol 94:1738–1744. https://doi.org/10.1002/jmv.27524

Schasfoort RBM (2017) Introduction to surface plasmon resonance. In: Schasfoort RBM (eds) Handbook of surface plasmon resonance, 2nd edn. The Royal Society of Chemistry, pp 1–26. https://doi.org/10.1039/9781788010283

Scholtissek C (1985) Stability of infectious influenza A viruses at low pH and at elevated temperature. Vaccine 3:215–218. https://doi.org/10.1016/0264-410X(85)90109-4

Shaik MM, Peng H, Lu J et al (2019) Structural basis of coreceptor recognition by HIV-1 envelope spike. Nature 565:318–323. https://doi.org/10.1038/s41586-018-0804-9

Shang J, Wan Y, Luo C et al (2020a) Cell entry mechanisms of SARS-CoV-2. Proc Natl Acad Sci U S A 117:11727–11734. https://doi.org/10.1073/pnas.2003138117

Shang J, Ye G, Shi K, Wan Y, Luo C, Aihara H, Geng Q, Auerbach A, Li F (2020b) Structural basis of receptor recognition by SARS-CoV-2. Nature 581:221–224. https://doi.org/10.1038/s41586-020-2179-y

Sharp PM, Hahn BH (2011) Origins of HIV and the AIDS pandemic. Cold Spring Harb Perspect Med 1:1–22. https://doi.org/10.1101/cshperspect.a006841

Shashkova S, Leake MC (2017) Single-molecule fluorescence microscopy review: shedding new light on old problems. Biosci Rep 37:1–19. https://doi.org/10.1042/BSR20170031

Shtyrya YA, Mochalova LV, Bovin NV (2009) Influenza virus neuraminidase structure and functions. Acta Nat 10:26–32. https://doi.org/10.3389/fmicb.2019.00039

Simon V, Ho DD, Abdool Karim Q (2006) HIV/AIDS epidemiology, pathogenesis, prevention, and treatment. Lancet 368:489–504. https://doi.org/10.1016/S0140-6736(06)69157-5

Simons K, Ikonen E (1997) Functional rafts in cell membranes. Nature 387:569–572. https://doi.org/10.1038/42408

Skehel JJ, Wiley DC (2000) Receptor binding and membrane fusion in virus entry: the influenza haemagglutinin. Annu Rev Biochem 69:531–569. https://doi.org/10.1101/cshperspect.a038778

Sood C, Marin M, Chande A et al (2017) SERINC5 protein inhibits HIV-1 fusion pore formation by promoting functional inactivation of envelope glycoproteins. J Biol Chem 292:6014–6026. https://doi.org/10.1074/jbc.M117.777714

Sood C, Marin M, Mason CS, Melikyan GB (2016) Visualization of content release from cell surface-attached single HIV-1 particles carrying an extra-viral fluorescent pH-sensor. PLoS ONE 11:1–19. https://doi.org/10.1371/journal.pone.0148944

Steffens CM, Hope TJ (2004) Mobility of the human immunodeficiency virus (HIV) receptor CD4 and coreceptor CCR5 in living cells: implications for HIV fusion and entry events. J Virol 78:9573–9578. https://doi.org/10.1128/jvi.78.17.9573-9578.2004

Straus MR, Bidon MK, Tang T, Jaimes JA, Whittaker GR, Daniel S (2021) Inhibitors of L-type calcium channels show therapeutic potential for treating SARS-CoV-2 infections by preventing virus entry and spread. ACS Infect Dis 7(10):2807–2815. https://doi.org/10.1021/acsinfecdis.1c00023

Suenaga E, Mizuno H, Kumar PKR (2012) Influenza virus surveillance using surface plasmon resonance. Virulence 3:464–470. https://doi.org/10.4161/viru.21822

Yang S-T, Kiessling V, Simmons JA, White JM, Tamm LK (2015) HIV gp41-mediated membrane fusion occurs at edges of cholesterol-rich lipid domains. Nat Chem Biol 11(6):424–431. https://doi.org/10.1038/nchembio.1800.HIV

Takemoto DK, Skehel JJ, Wiley DC (1996) A surface plasmon resonance assay for the binding of influenza virus hemagglutinin to its sialic acid receptor. Virology 217:452–458. https://doi.org/10.1006/viro.1996.0139

Tandon R, Sharp JS, Zhang F et al (2021) Effective inhibition of SARS-CoV-2 entry by heparin and enoxaparin derivatives. J Virol 95:1–12. https://doi.org/10.1128/jvi.01987-20

Tang T, Bidon M, Jaimes JA et al (2020) Coronavirus membrane fusion mechanism offers a potential target for antiviral development. Antiviral Res 178:1–17. https://doi.org/10.1016/j.antiviral.2020.104792

Tang T, Jaimes JA, Bidon MK et al (2021) Proteolytic activation of SARS-CoV-2 spike at the S1/S2 boundary: potential role of proteases beyond furin. ACS Infect Dis 7:264–272. https://doi.org/10.1021/acsinfecdis.0c00701

Taylor PC, Adams AC, Hufford MM et al (2021) Neutralizing monoclonal antibodies for treatment of COVID-19. Nat Rev Immunol 21:382–393. https://doi.org/10.1038/s41577-021-00542-x

Tran EEH, Borgnia MJ, Kuybeda O, Schauder DM, Bartesaghi A, Frank GA, Sapira G, Milne JLS, Subramaniam S (2012) Structural mechanism of trimeric HIV-1 envelope glycoprotein activation. PLoS Pathog 8(7):e1002797. https://doi.org/10.1371/journal.ppat.1002797

Trautz B, Wiedemann H, Lüchtenborg C et al (2017) The host-cell restriction factor SERINC5 restricts HIV-1 infectivity without altering the lipid composition and organization of viral particles. J Biol Chem 292:13702–13713. https://doi.org/10.1074/jbc.M117.797332

V'kovski P, Kratzel A, Steiner S et al (2021) Coronavirus biology and replication: implications for SARS-CoV-2. Nat Rev Microbiol 19:155–170. https://doi.org/10.1038/s41579-020-00468-6

Varghese JN, Colman PM (1991) Three-dimensional structure of the negraminidase of influenza virus A/Tokyo/3/67 at 2–2 A resolution receptor. J Mol Biol 2211:473–486. https://doi.org/10.1016/0022-2836(91)80068-6

Varghese J, Laver W, Coman P (1983) Structure of the influenza virus glycoprotein antigen neuraminidase at 2.9 Å resolution. Nature 303:35–40. https://doi.org/10.1038/303035a0

Vijayakrishnan S, Loney C, Jackson D et al (2013) Cryotomography of budding influenza A virus reveals filaments with diverse morphologies that mostly do not bear a genome at their distal end. PLoS Pathog 9:1–11. https://doi.org/10.1371/journal.ppat.1003413

Villamil Giraldo AM, Kasson PM (2020) Bilayer-coated nanoparticles reveal how influenza viral entry depends on membrane deformability but not curvature. J Phys Chem Lett 11:7190–7196. https://doi.org/10.1021/acs.jpclett.0c01778

Walls AC, Park YJ, Tortorici MA et al (2020) Structure, function, and antigenicity of the SARS-CoV-2 spike glycoprotein. Cell 181:281-292.e6. https://doi.org/10.1016/j.cell.2020.02.058

Walls AC, Tortorici MA, Bosch BJ et al (2016) Cryo-electron microscopy structure of a coronavirus spike glycoprotein trimer. Nature 531:114–117. https://doi.org/10.1038/nature16988

Wang H, Yuan Z, Pavel MA et al (2021) The role of high cholesterol in age-related COVID19 lethality. BioRxiv 15:1–14. https://doi.org/10.1101/2020.05.09.086249

Wang Q, Zhang Y, Wu L et al (2020) Structural and functional basis of SARS-CoV-2 entry by using human ACE2. Cell 181:894–904. https://doi.org/10.1016/j.cell.2020.03.045

Ward AE, Kiessling V, Pornillos O et al (2020) HIV-cell membrane fusion intermediates are restricted by Serincs as revealed by cryo-electron and TIRF microscopy. J Biol Chem 295:15183–15195. https://doi.org/10.1074/jbc.RA120.014466

Watanabe Y, Allen JD, Wrapp D et al (2020) Site-specific glycan analysis of the SARS-CoV-2 spike. Science 369(80):330–333. https://doi.org/10.1126/science.abb9983

Weis W, Brown JH, Cusack S, Paulson JC, Skehel JJ, Wiley DC (1988) Structure of the influenza virus haemagglutinin complexed with its receptor, sialic acid. Nature 333(6172):426–431. https://doi.org/10.1038/333426a0

Weis WI, Brünger AT, Skehel JJ, Wiley DC (1990) Refinement of the influenza virus hemagglutinin by simulated annealing. J Mol Biol 212:737–761. https://doi.org/10.1016/0022-2836(90)90234-D

Weissenhorn W, Dessen A, Harrison SC et al (1997) Atomic structure of the ectodomain from HIV-1 gp41. Nature 387:426–430. https://doi.org/10.1038/387426a0

White JM, Whittaker GR (2016) Fusion of enveloped viruses in endosomes. Traffic 17:593–614. https://doi.org/10.1111/tra.12389

Whittaker GR (2021) SARS-CoV-2 spike and its adaptable furin cleavage site. The Lancet Microbe 2:488–489. https://doi.org/10.1016/S2666-5247(21)00174-9

Wilen CB, Tilton JC, Doms RW (2012) HIV: cell binding and entry. Cold Spring Harb Perspect Med 2(8):a006866. https://doi.org/10.1101/cshperspect.a006866

Wilson IA, Skehel JJ, Wiley D (1981) Structure of the haemagglutinin membrane glycoprotein of influenza virus at 3Å resolution. Nature 289:367–373. https://doi.org/10.1038/289366a0

Wrapp D, Wang N, Corbett KS et al (2020) Cryo-EM structure of the 2019-nCoV spike in the prefusion conformation. Science 367(80):1260–1263. https://doi.org/10.1126/science.aax0902

Wu A, Peng Y, Huang B et al (2020) Genome composition and divergence of the novel coronavirus (2019-nCoV) originating in China. Cell Host Microbe 27:325–328. https://doi.org/10.1016/j.chom.2020.02.001

Xia S, Lan Q, Su S (2020a) The role of furin cleavage site in SARS-CoV-2 spike protein-mediated membrane fusion in the presence or absence of trypsin. Sig Transduct Target Ther 5:92. https://doi.org/10.1038/s41392-020-0184-0

Xia S, Liu M, Wang C et al (2020b) Inhibition of SARS-CoV-2 (previously 2019-nCoV) infection by a highly potent pan-coronavirus fusion inhibitor targeting its spike protein that harbors a high capacity to mediate membrane fusion. Cell Res 30:343–355. https://doi.org/10.1038/s41422-020-0305-x

Xiong X, Coombs PJ, Martin SR et al (2013) Receptor binding by a ferret-transmissible H5 avian influenza virus. Nature 497:392–396. https://doi.org/10.1038/nature12144

Yamaguchi M, Danev R, Nishiyama K et al (2008) Zernike phase contrast electron microscopy of ice-embedded influenza A virus. J Struct Biol 162:271–276. https://doi.org/10.1016/j.jsb.2008.01.009

Yang J, Petitjean SJL, Koehler M et al (2020) Molecular interaction and inhibition of SARS-CoV-2 binding to the ACE2 receptor. Nat Commun 11:1–10. https://doi.org/10.1038/s41467-020-18319-6

Yang S-T, Kiessling V, Tamm LK (2016) Line tension at lipid phase boundaries as driving force for HIV fusion peptide-mediated fusion. Nat Commun 7:11401. https://doi.org/10.1038/ncomms11401

Yang ST, Kreutzberger AJB, Kiessling V et al (2017) HIV virions sense plasma membrane heterogeneity for cell entry. Sci Adv 3:1–13. https://doi.org/10.1126/sciadv.1700338

Yu M, Zhang T, Zhang W et al (2021) Elucidating the interactions between heparin/heparan sulfate and SARS-CoV-2-related proteins—an important strategy for developing novel therapeutics for the COVID-19 pandemic. Front Mol Biosci 7:1–13. https://doi.org/10.3389/fmolb.2020.628551

Zang R, Case JB, Yutuc E et al (2020) Cholesterol 25-hydroxylase suppresses SARS-CoV-2 replication by blocking membrane fusion. Proc Natl Acad Sci U S A 117:32105–32113. https://doi.org/10.1073/pnas.2012197117

Zaraket H, Bridges OA, Russell CJ (2013) The pH of activation of the hemagglutinin protein regulates H5N1 influenza virus replication and pathogenesis in mice. J Virol 87:4826–4834. https://doi.org/10.1128/jvi.03110-12

Zhang J, Cai Y, Xiao T et al (2021) Structural impact on SARS-CoV-2 spike protein by D614G substitution. Science 372(80):525–530. https://doi.org/10.1126/science.abf2303

Zhang J, Pekosz A, Lamb RA (2000) Influenza virus assembly and lipid raft microdomains: a role for the cytoplasmic tails of the spike glycoproteins. J Virol 74:4634–4644. https://doi.org/10.1128/jvi.74.10.4634-4644.2000

Zhang X, Zhou T, Yang J et al (2017) Identification of SERINC5-001 as the predominant spliced isoform for HIV-1 restriction. J Virol 91:1–13. https://doi.org/10.1128/jvi.00137-17

Zhdanov VP (2021) Virology from the perspective of theoretical colloid and interface science. Curr Opin Colloid Interface Sci 53:1–9. https://doi.org/10.1016/j.cocis.2021.101450

Zhdanov VP, Höök F (2015) Diffusion-limited attachment of large spherical particles to flexible membrane-immobilized receptors. Eur Biophys J 44:219–226. https://doi.org/10.1007/s00249-015-1016-y

Zhou P, Lou YX, Wang XG et al (2020) A pneumonia outbreak associated with a new coronavirus of probable bat origin. Nature 579:270–273. https://doi.org/10.1038/s41586-020-2012-7

Zhu P, Liu J, Bess J et al (2006) Distribution and three-dimensional structure of AIDS virus envelope spikes. Nature 441:847–852. https://doi.org/10.1038/nature04817

Zhu Z-L, Qiu X-D, Wu S et al (2021) Blocking effect of demethylzeylasteral on the interaction between human ACE2 protein and SARS-CoV-2 RBD protein discovered using SPR technology. Molecules 26:1–12. https://doi.org/10.3390/molecules26010057

Zlatanova J, Lindsay SM, Leuba SH (2000) Single molecule force spectroscopy in biology using the atomic force microscope. Prog Biophys Mol Biol 74:37–61. https://doi.org/10.1016/s0079-6107(00)00014-6